LOFAR Deep Fields: Probing the sub-mJy regime of polarized extragalactic sources in ELAIS-N1

Sara Piras
Chalmers University of Technology
Onsala Space Observatory
Sweden

In collaboration with: C. Horellou, J. E. Conway, M. Thomasson, S. del Palacio, T. W. Shimwell, S. P. O'Sullivan, E. Carretti, I. Šnidaric´, V. Jelic´, B. Adebahr, A. Berger, P. N. Best, M. Brüggen, N. Herrera Ruiz, R. Paladino, I. Prandoni, J. Sabater, and V. Vacca

2nd National SKA Science Day, Gothenburg

10 -11th of September, 2024

OUTLINE

- Introduction
- Paper I: The catalog, 2024, A&A, accepted
- Paper II: Analysis, 2024, submitted to A&A
- Summary and Outlook

Probing Extragalactic Magnetic Fields

X-ray, Optical & Radio Images of Cygnus A. Credits: https://chandra.cfa.harvard.edu/photochronological15.html

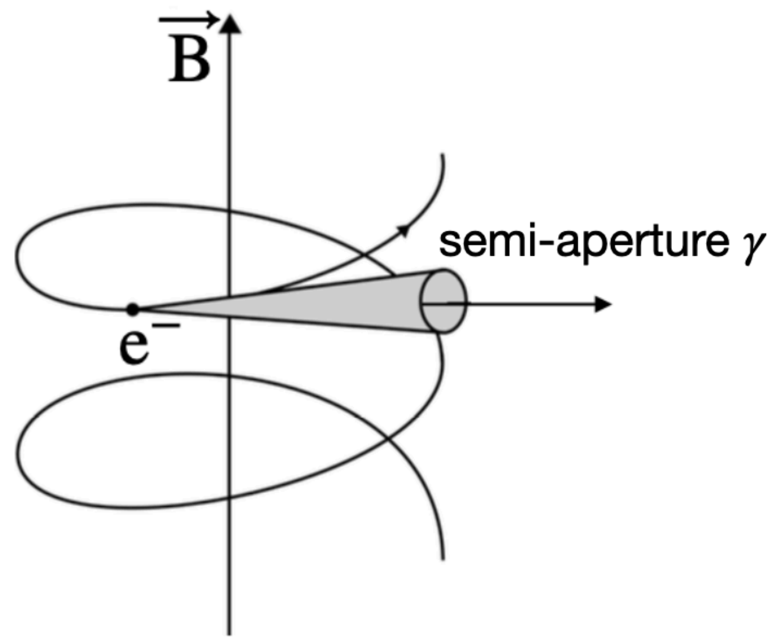

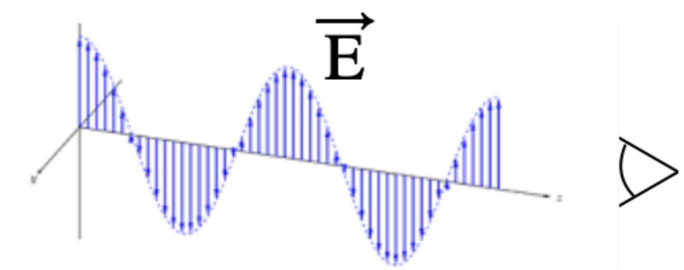

Linearly polarized radiation

Extragalactic radio sources:
- Radio galaxy
- Blazar
- Quasar

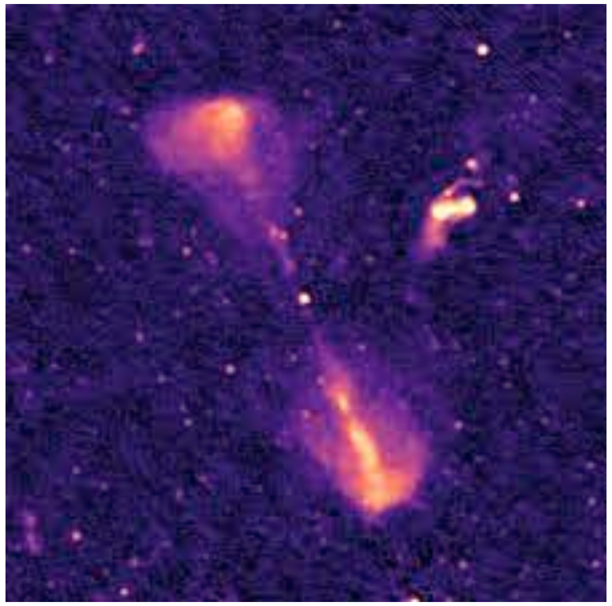

Radio galaxy observed at 150 MHz (ELAIS- N1 LOFAR Deep Field, Sabater et al. 2021)

Probing Extragalactic Magnetic Fields

X-ray, Optical & Radio Images of Cygnus A. Credits: https://chandra.cfa.harvard.edu/photochronological15.html

Magneto-ionic medium

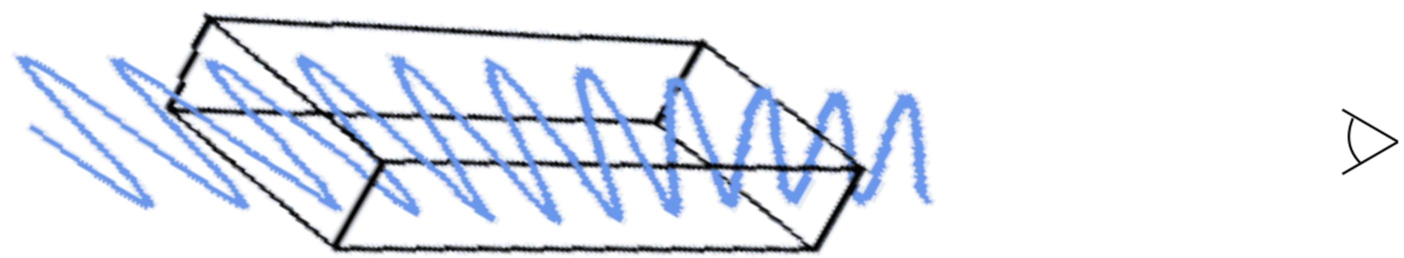

Faraday rotation of a linearly polarized emission

Faraday rotation **of linearly polarized background emission due to magneto-ionic media along the line of sight reveals indirectly magnetic fields at radio wavelengths**

Faraday rotation

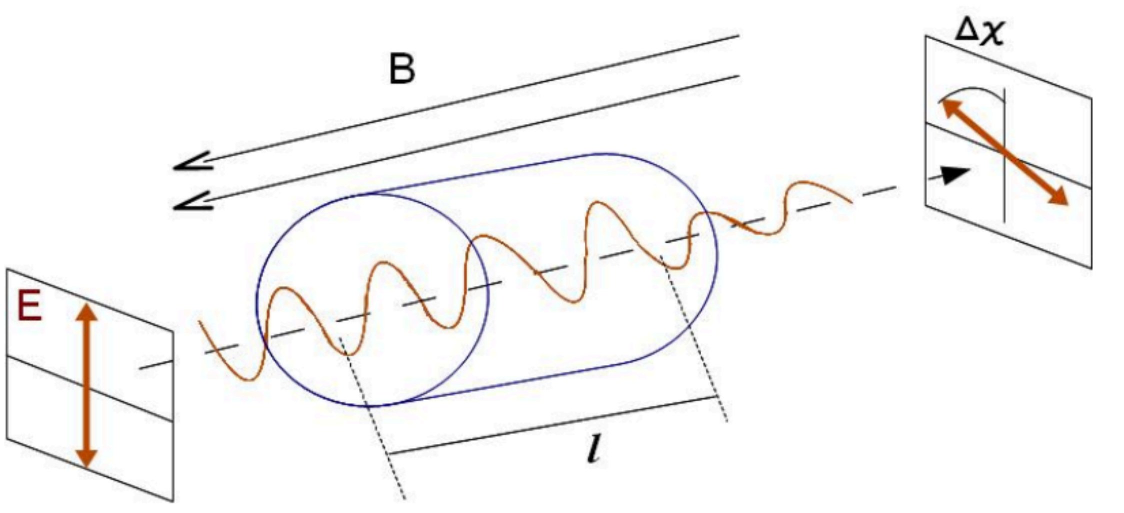

Faraday rotation causes the intrinsic polarization angle of polarized emission to rotate as it propagates through a magneto-ionic medium

$$\chi(\lambda^2) = \chi_0 + \mathrm{RM}\lambda^2$$

RM = rotation measure

For a synchrotron-emitting source behind a magneto-ionic medium:

$\boxed{\mathrm{RM} = \phi}$

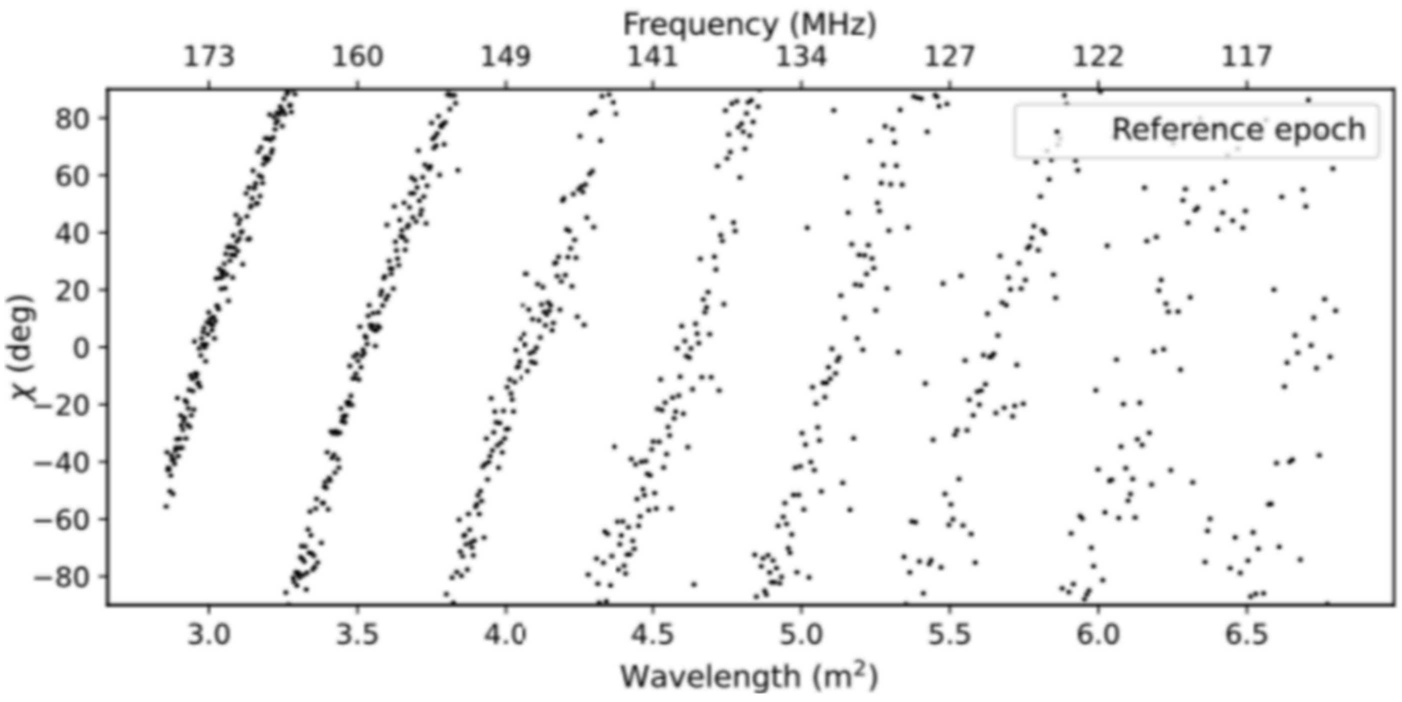

Piras et al. 2024

$$\boxed{\phi} = 0.81 \int_{source}^{observer} \frac{B_{\parallel}}{(\mu G)} \frac{n_e}{cm^{-3}} \frac{dl}{pc} \ \ \mathrm{rad\ m^{-2}}$$ Faraday depth

Rotation measure (RM) grid

1.4 GHz, ~30 000 deg²

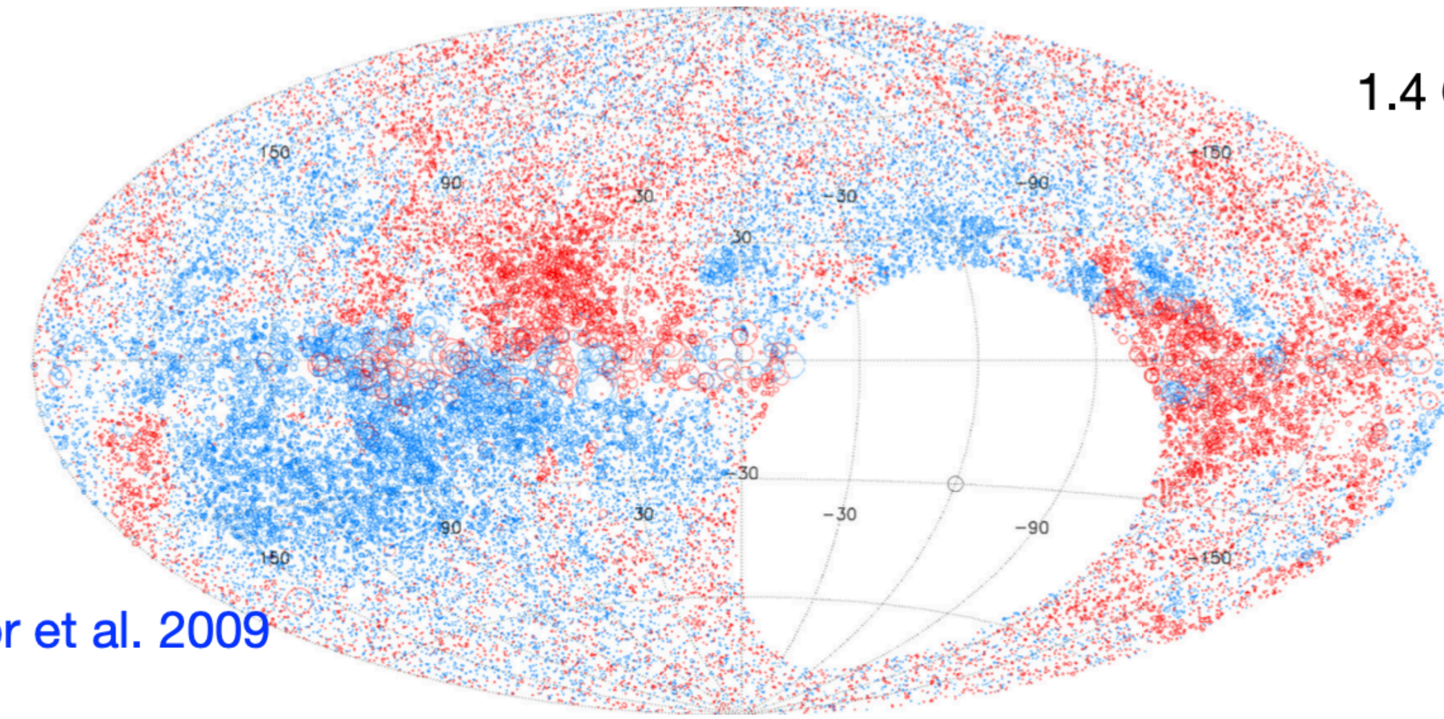

Taylor et al. 2009

Hutschenreuter et al. 2022

150 MHz, ~6000 deg²

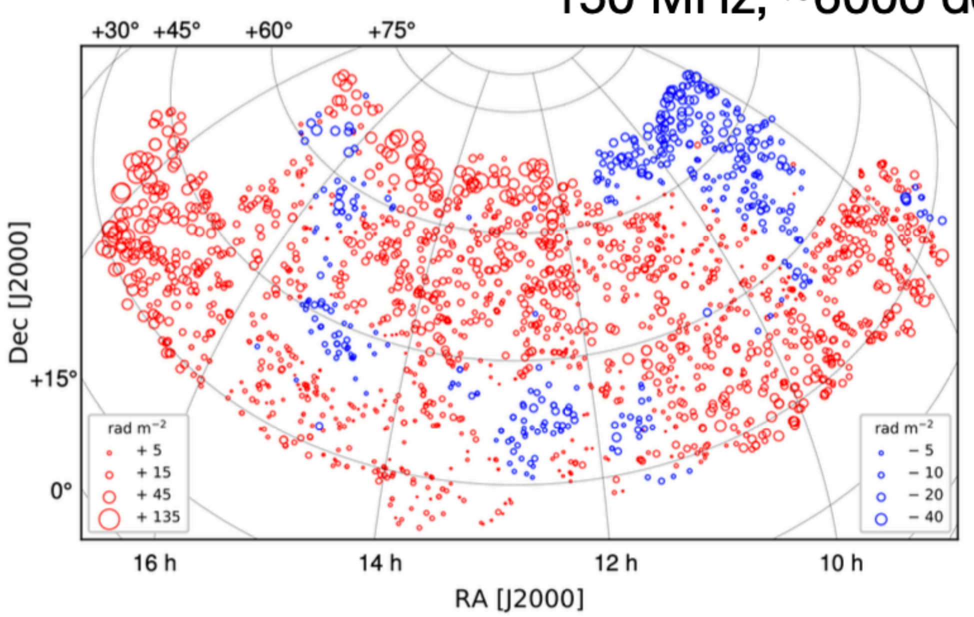

O'Sullivan et al. 2023

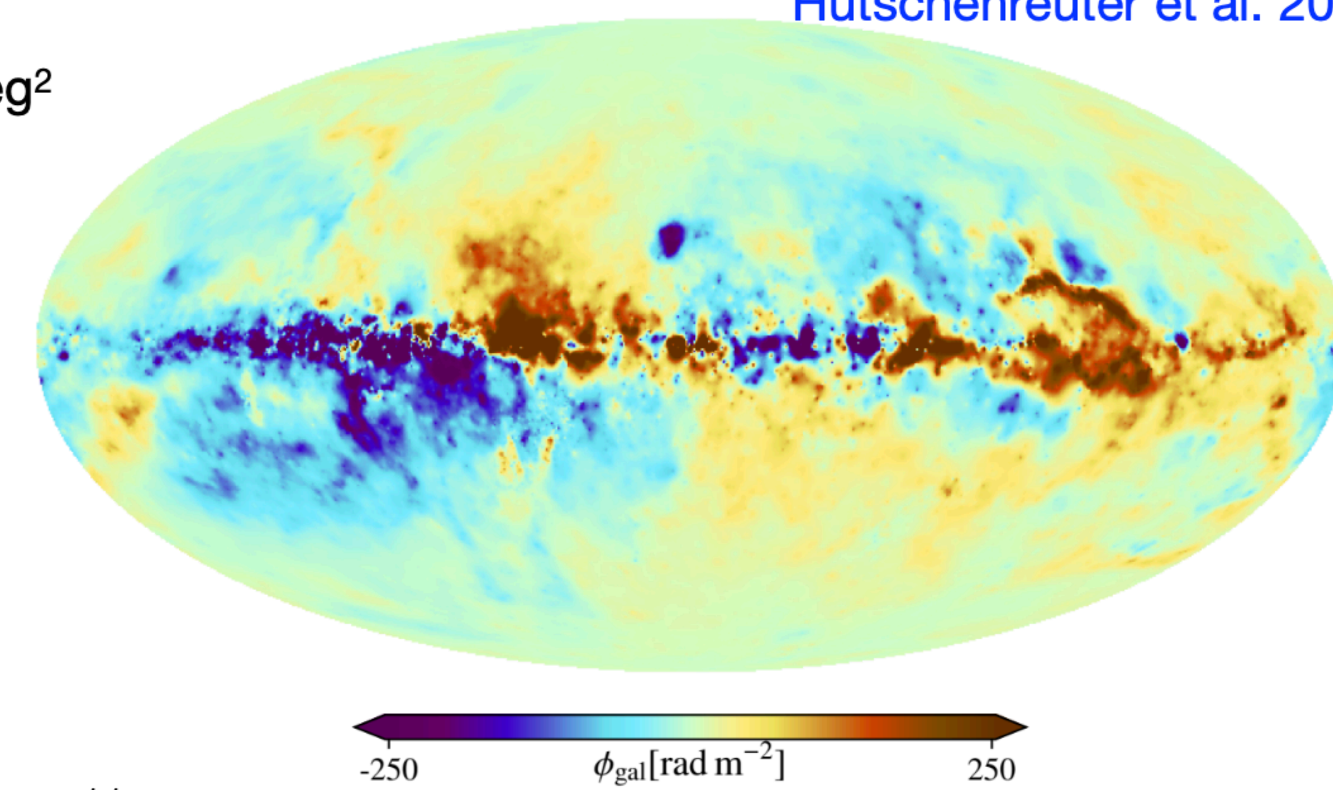

The LOw Frequency ARray (LOFAR)

- Observing at <200 MHz
- Small antennas, mainly in the Netherlands
- International stations
- Will cover the entire northern sky

LOFAR Two-metre Sky Survey (LoTSS) 8 h observation per pointing		
	Resolution	Sensitivity
Stokes I	6 arcsec	~100 μJy/b
	20 arcsec	~500 μJy/b
Stokes Q,U	4 arcmin	~1 mJy/b
	20 arcsec	~100 μJy/b

The LOFAR station in Netherlands. Credits: https://www.astron.nl/

LOFAR station in Onsala. Credits:Onsala Space Observatory/R. Hammargren

- LOFAR-VLBI → 0.3” arcsec resolution

Polarization with LOFAR

- Frequency range of HBA: ≈120 - 168 MHz (wavelengths of 1.8 - 2.5 m)
- High precision on rotation measures: ~1 rad/m^2
- But stronger Faraday depolarization at long wavelengths
- Polarized counts are unknown at low frequencies

Polarized sources per square degree	Resolution	Noise level	Field
0.16	4.3'	1 mJy/beam	HETDEX DR1 Van Eck et al. 2018
0.3	20"	100 μJy/beam	M51 Neld et al. 2018
0.6	20"	26 μJy/beam	ELAIS-N1 Herrera Ruiz et al. 2021
0.4	20"	80 μJy/beam	LoTSS DR2 O'Sullivan et al. 2023

How to increase the number of polarized sources detected low frequency?

The ELAIS-N1 LOFAR deep field

- European Large Area ISO Survey-North 1
- Multiwavelength coverage: optical, infrared, radio
- With LOFAR (HBA at 114.9-177.4 MHz, 1.69-2.61 m): Sabater et al. 2021
  - 22 available epochs of 8 h each = 176 h
  - In Stokes I: final sensitivity of ~20 μJy/beam (central region), resolution of 6", 68 deg^2
  - ~80 000 sources detected in continuum (~3 000 above 1 mJy/beam) Kondapally et al. 2021
    - ~30 000 host-galaxies in ~7.15 deg^2 Redshifts Duncan et al. 2021

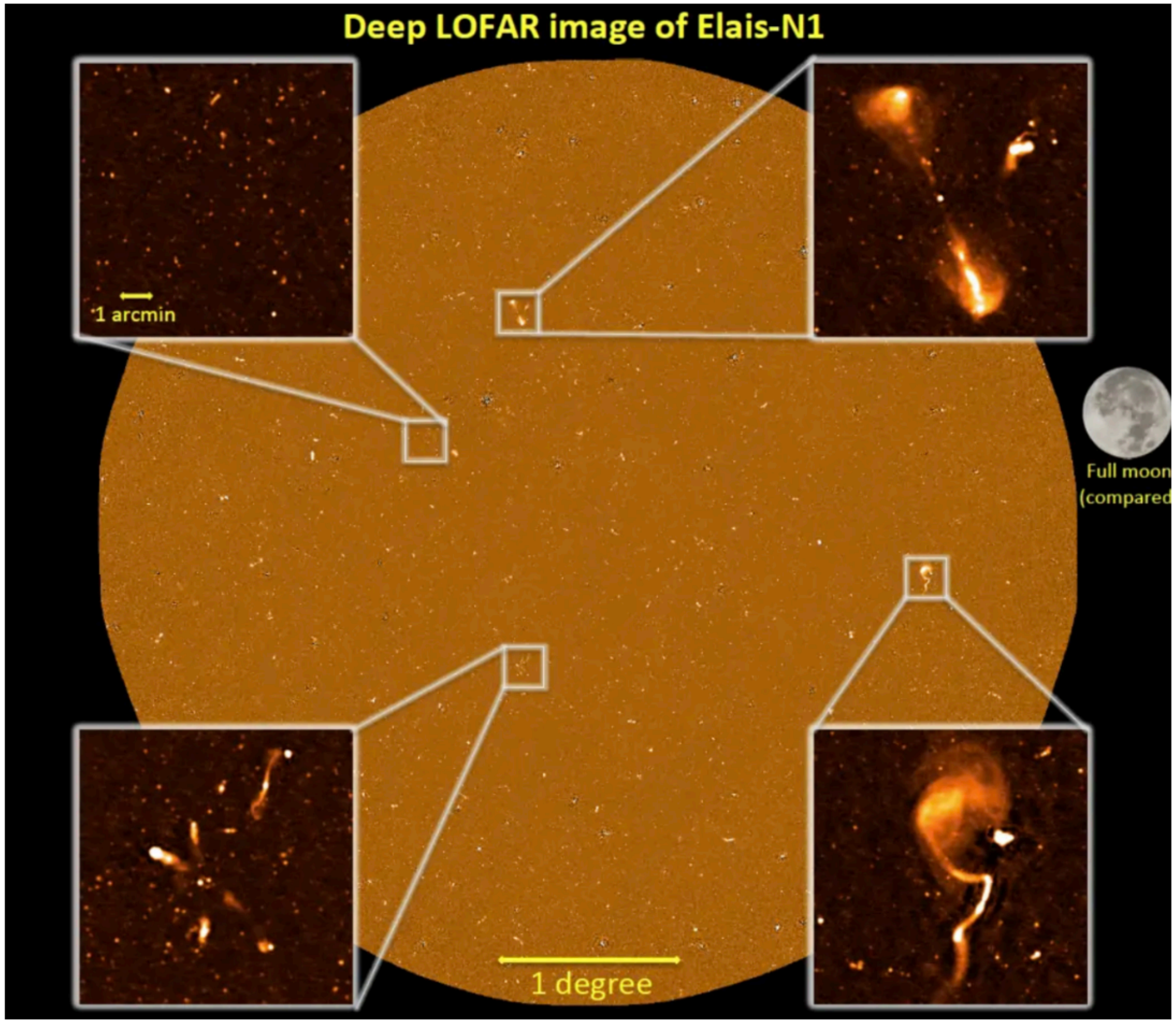

Philip Best & Jose Sabater, University of Edinburgh

PAPER I. THE CATALOG

- 25 deg² region
- Deepest polarimetric study at lowest frequencies
  - Highest resolution (6”)
  - 19 8-hour-long epochs combined
    - Lowest noise level of 19 μJy beam^{-1}
  - Algorithm to process and analyze tens of TB

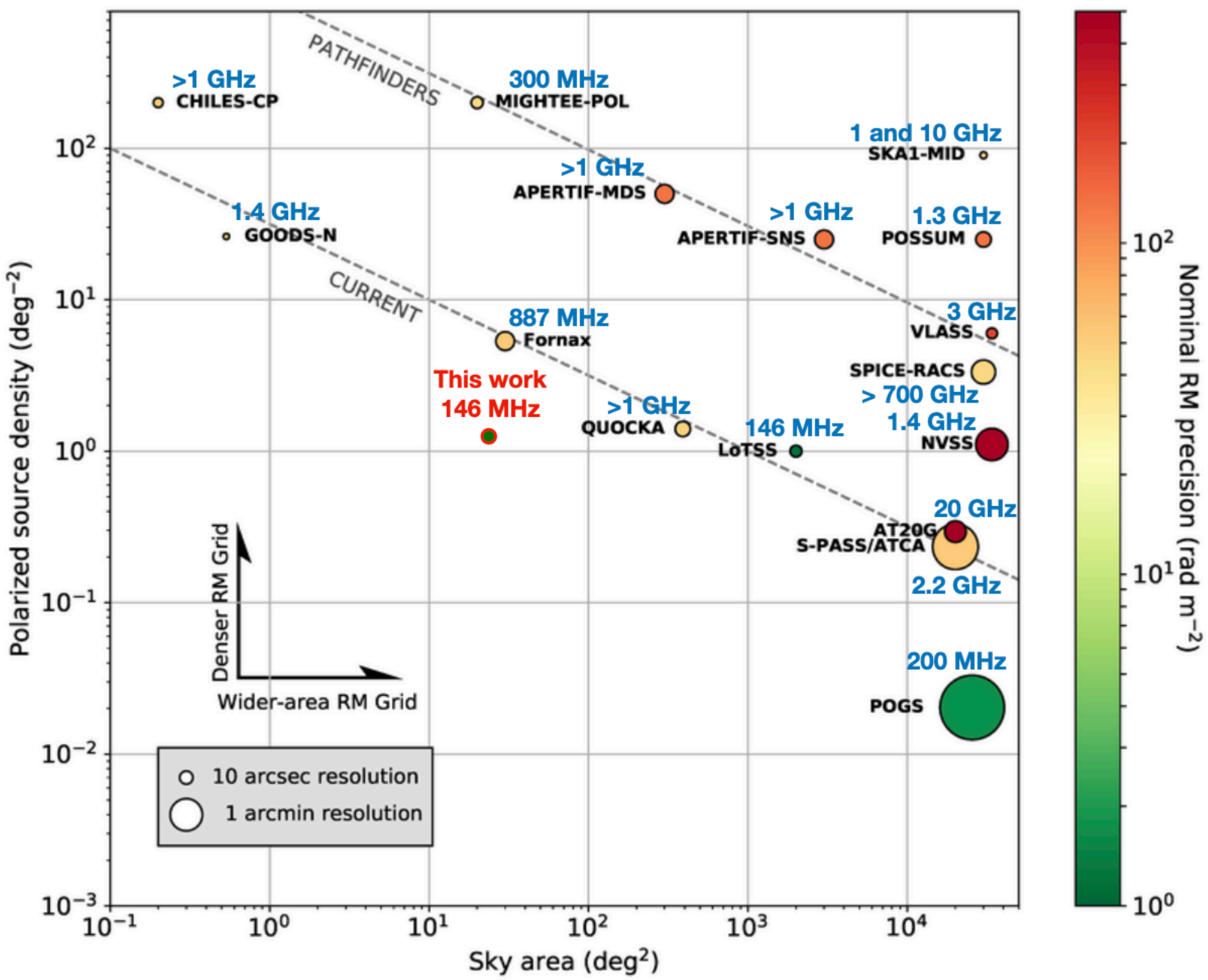

Adapted from Heald et al. 2020

- **Stacking**

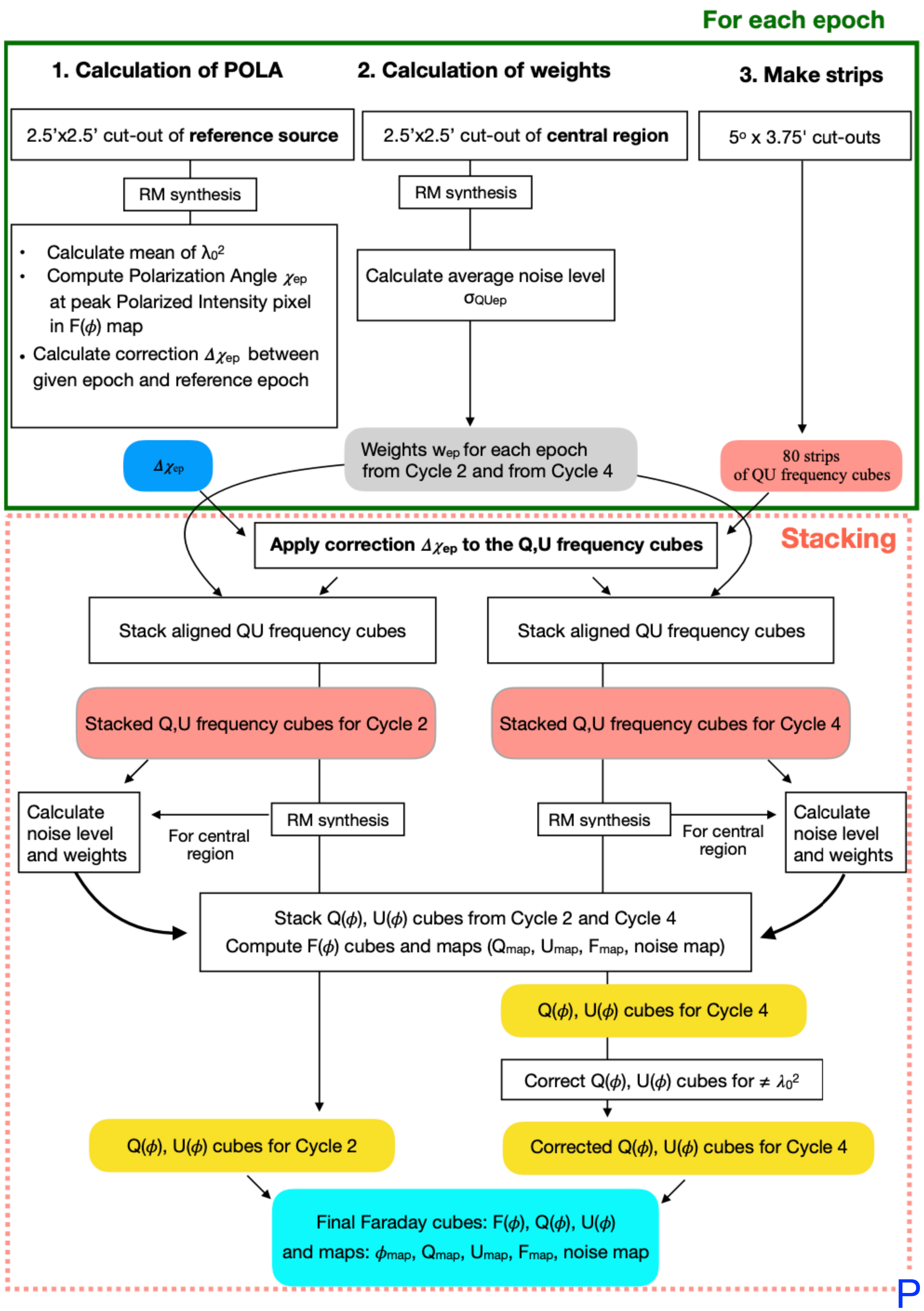

Piras et al. 2024

Fig. 2: Flowchart of the stacking process. POLA stands for Polarization Angle.

Polarization in ELAIS-N1

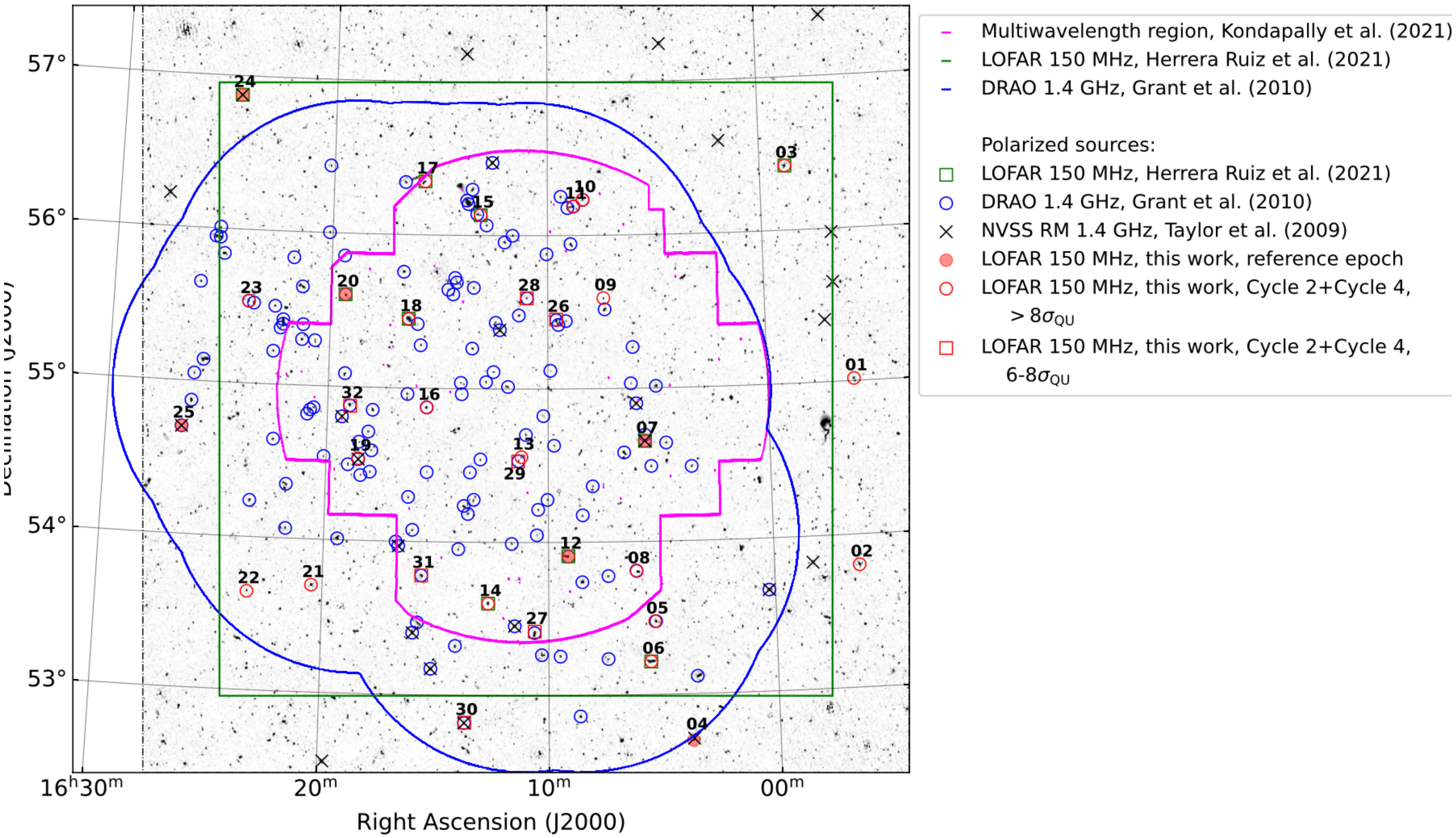

Table 1: Basic characteristics of polarization studies covering the ELAIS-N1 field.

Catalog	Reference	Frequency	Sensitivity in Q and U (μJy beam^{-1})	Resolution (arcsec)	Area (deg^2)	Number of polarized sources	
NVSS RM	(1)	1.4 GHz	290	45	25	25	Taylor et al. 2009
DRAO ELAIS-N1	(2)	1.4 GHz	78	49×59	7.43	83	Taylor et al. 2007
DRAO ELAIS-N1	(3)	1.4 GHz	45	49×62	15.16	136	Grant et al. 2010
LOFAR	(4)	150 MHz	26	20	16	10	Herrera Ruiz et al. 2021
LOFAR	(5)	150 MHz	22	6	25	31	Piras et al. 2024

PAPER I. THE CATALOG

- **33 polarized components from 31 radio galaxies**
  - **26 components above 8σ_{QU}**
  - **7 components between 6-8σ_{QU}**

Table 6: Catalog of polarized sources in the ELAIS-N1 field detected with LOFAR.

Source ID (1)	LOFAR ID (2)	RA (J2000) (deg) (3)	Dec (J2000) (deg) (4)	P_p (mJy beam^{-1}) (5)	RM (rad m^{-2}) (6)	I_p (mJy beam^{-1}) (7)	Π (%) (8)	Pol. info (9)
$01^{(b,c)}$	ILTJ155603.98+550056.8	239.0149	55.0158	1.02	1.68 ± 0.02	59.15	1.72	
02	ILTJ155614.81+534814.8	239.0612	53.8012	0.54	9.71 ± 0.05	76.83	0.71	
$03^{(b,c)}$	ILTJ155848.42+562514.4	239.7013	56.4209	1.19	-5.83 ± 0.02	187.98	0.64	3
$04_{A}^{(a,b,c)}$	ILTJ160344.42+524228.0	240.9436	52.6961	2.69	19.68 ± 0.01	135.80	1.98	2
$04_{B}^{(a,b,c)}$	ILTJ160344.42+524228.0	240.9283	52.7150	9.07	21.78 ± 0.01	205.02	4.43	2
05	ILTJ160520.16+532837.2	241.3342	53.4771	0.33	19.12 ± 0.05	39.30	0.86	1
$06^{(b,c)}$	ILTJ160532.84+531257.4	241.3853	53.2159	0.66	18.43 ± 0.03	19.41	3.42	3
$07^{(a,b,c)}$	**ILTJ160538.33+543922.6**	241.4080	54.6551	6.23	6.062 ± 0.003	355.62	1.75	1,2,3
$08^{(c)}$	ILTJ160603.11+534812.6	241.5271	53.8078	0.39	13.39 ± 0.03	48.38	0.82	1
$09^{(b)}$	ILTJ160725.85+553525.8	241.8578	55.5905	0.38	-3.79 ± 0.03	16.87	2.27	
10	ILTJ160820.72+561355.7	242.0866	56.2325	0.24	-5.61 ± 0.05	54.61	0.45	1
11	ILTJ160847.74+561119.0	242.1929	56.1893	0.28	-6.24 ± 0.04	38.32	0.75	1
$12^{(a,b,c)}$	ILTJ160908.39+535425.4	242.2803	53.9090	0.72	7.17 ± 0.02	18.68	3.86	1,3
$13_{A}^{(c)}$	ILTJ161112.81+543317.5	242.8025	54.5562	0.25	2.38 ± 0.04	3.77	6.62	
$14^{(b,c)}$	ILTJ161240.15+533558.3	243.1678	53.5991	0.61	10.31 ± 0.02	33.66	1.82	3
$15^{(b)}$	ILTJ161314.05+560810.8	243.2816	56.1327	0.32	-4.80 ± 0.04	2.18	14.76	1,3
16	ILTJ161529.67+545235.2	243.8747	54.8748	0.20	-4.01 ± 0.05	3.85	5.17	1
$17^{(b,c)}$	ILTJ161548.36+562030.1	243.9344	56.3492	0.53	1.95 ± 0.03	9.19	5.77	3
$18^{(b,c)}$	ILTJ161623.79+552700.8	244.0991	55.4505	0.36	-20.31 ± 0.03	9.00	4.07	1,3
$19^{(b)}$	ILTJ161832.97+543146.3	244.6383	54.5344	0.30	2.91 ± 0.04	39.22	0.77	1,2
$20^{(a,b,c)}$	ILTJ161919.70+553556.7	244.8332	55.6012	0.51	-4.7 ± 0.02	33.55	1.52	1,3
21	ILTJ162027.55+534208.8	245.1212	53.7011	0.43	3.29 ± 0.04	76.11	0.57	
$22^{(b)}$	ILTJ162318.64+533847.4	245.8280	53.6447	0.54	2.31 ± 0.05	13.24	4.14	
23	ILTJ162347.10+553207.2	245.9442	55.5346	0.36	5.91 ± 0.05	15.10	2.39	1
$24^{(a,b,c)}$	ILTJ162432.20+565228.5	246.1343	56.8748	6.22	9.43 ± 0.01	138.47	4.50	2,3
$25^{(a,b,c)}$	ILTJ162634.18+544207.8	246.6426	54.7020	0.97	10.03 ± 0.02	71.80	1.35	1,2
26	ILTJ160936.45+552659.0	242.4032	55.4533	0.15	-5.38 ± 0.07	10.17	1.55	1
27	ILTJ161037.49+532425.1	242.6549	53.4177	0.22	14.17 ± 0.07	3.18	7.02	1
$28^{(b,c)}$	ILTJ161057.72+553527.9	242.7404	55.5913	0.20	-5.74 ± 0.05	36.72	0.56	1
$29^{(c)}$ (13_{B})	ILTJ161120.73+543147.7	242.8390	54.5283	0.19	3.92 ± 0.05	8.62	2.19	1
30	ILTJ161340.99+524913.0	243.4168	52.8230	0.32	19.4 ± 0.07	29.41	1.11	1
$31^{(b,c)}$	ILTJ161537.86+534646.4	243.9072	53.7797	0.24	6.23 ± 0.06	18.50	1.32	1
32	ILTJ161859.41+545246.3	244.7448	54.8745	0.18	-4.05 ± 0.06	23.05	0.82	1

Piras et al. 2024

PAPER I. THE CATALOG

- **WIDE (LoTSS DR2) vs DEEP (this work)**

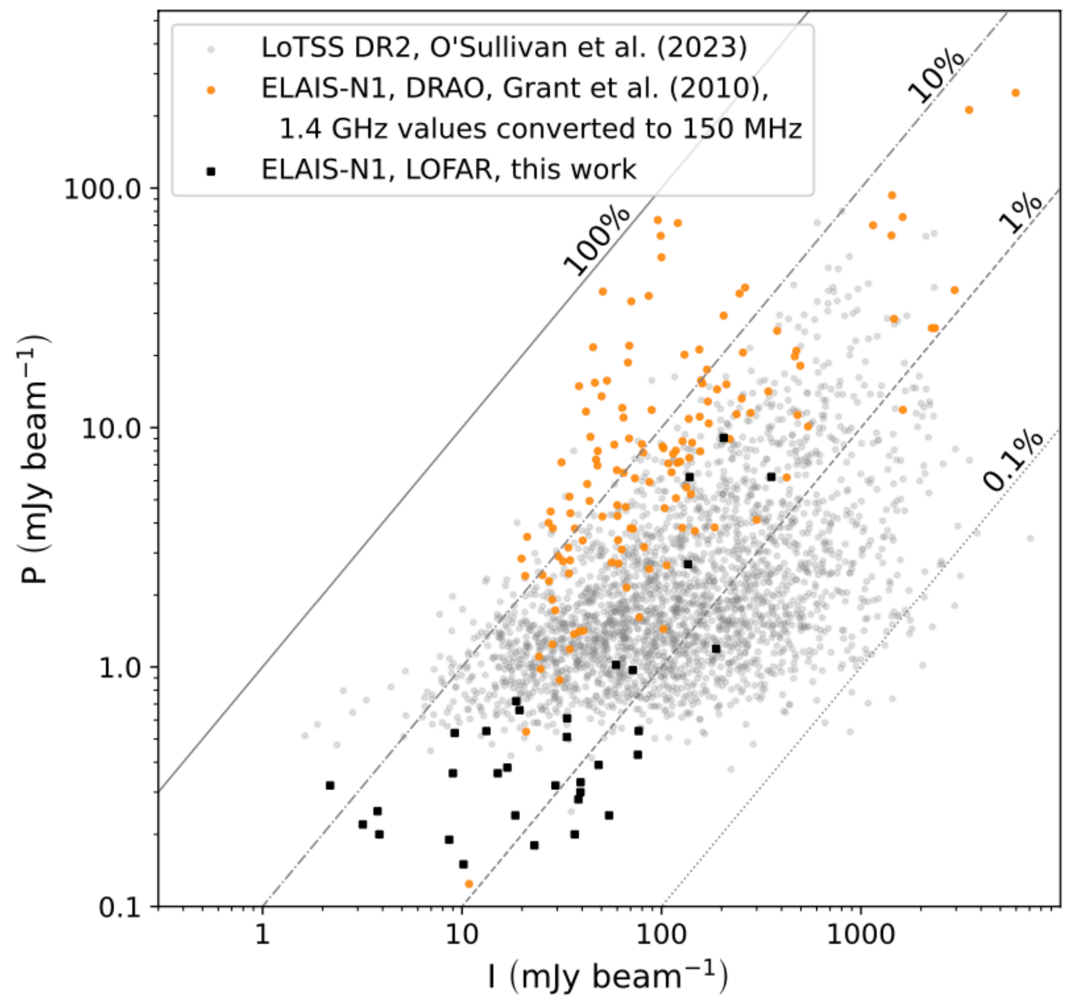

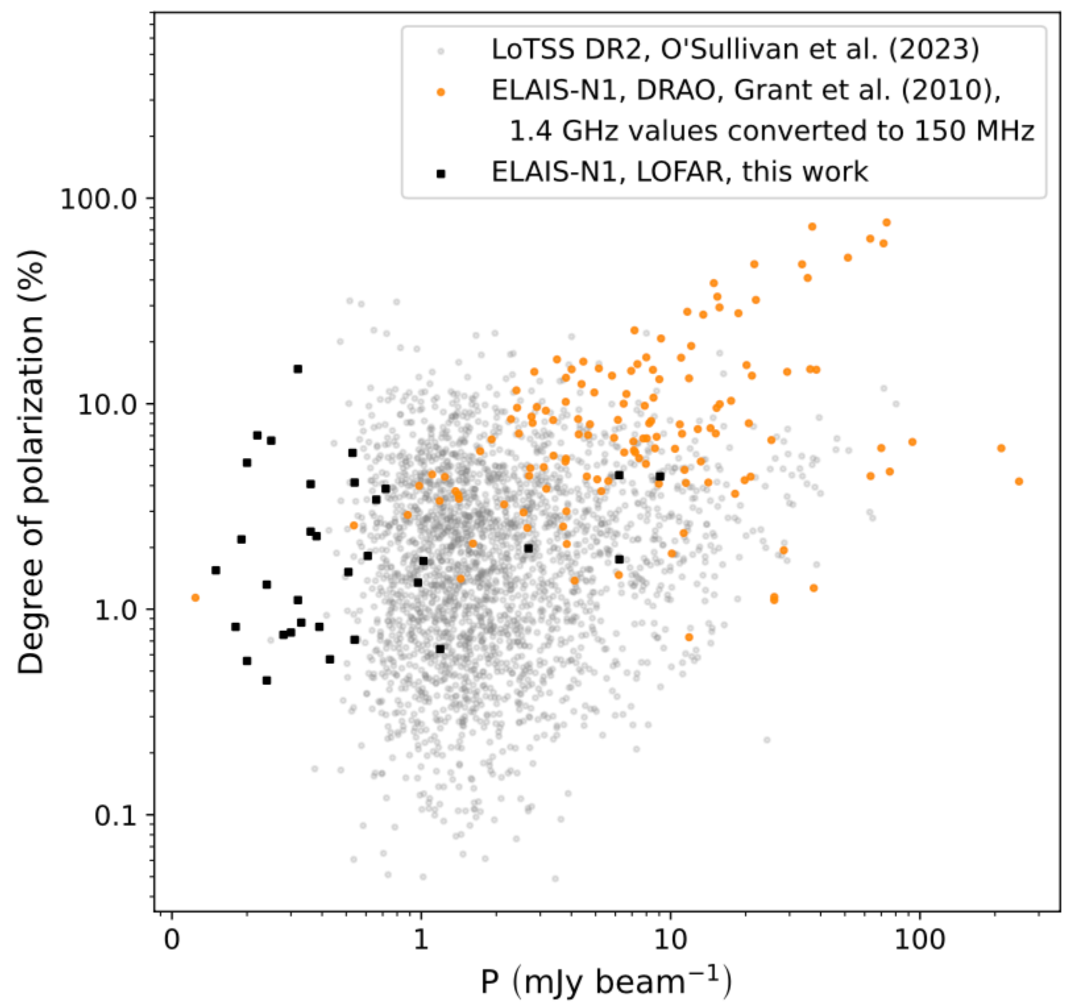

Piras et al. 2024

- **Polarized source counts**

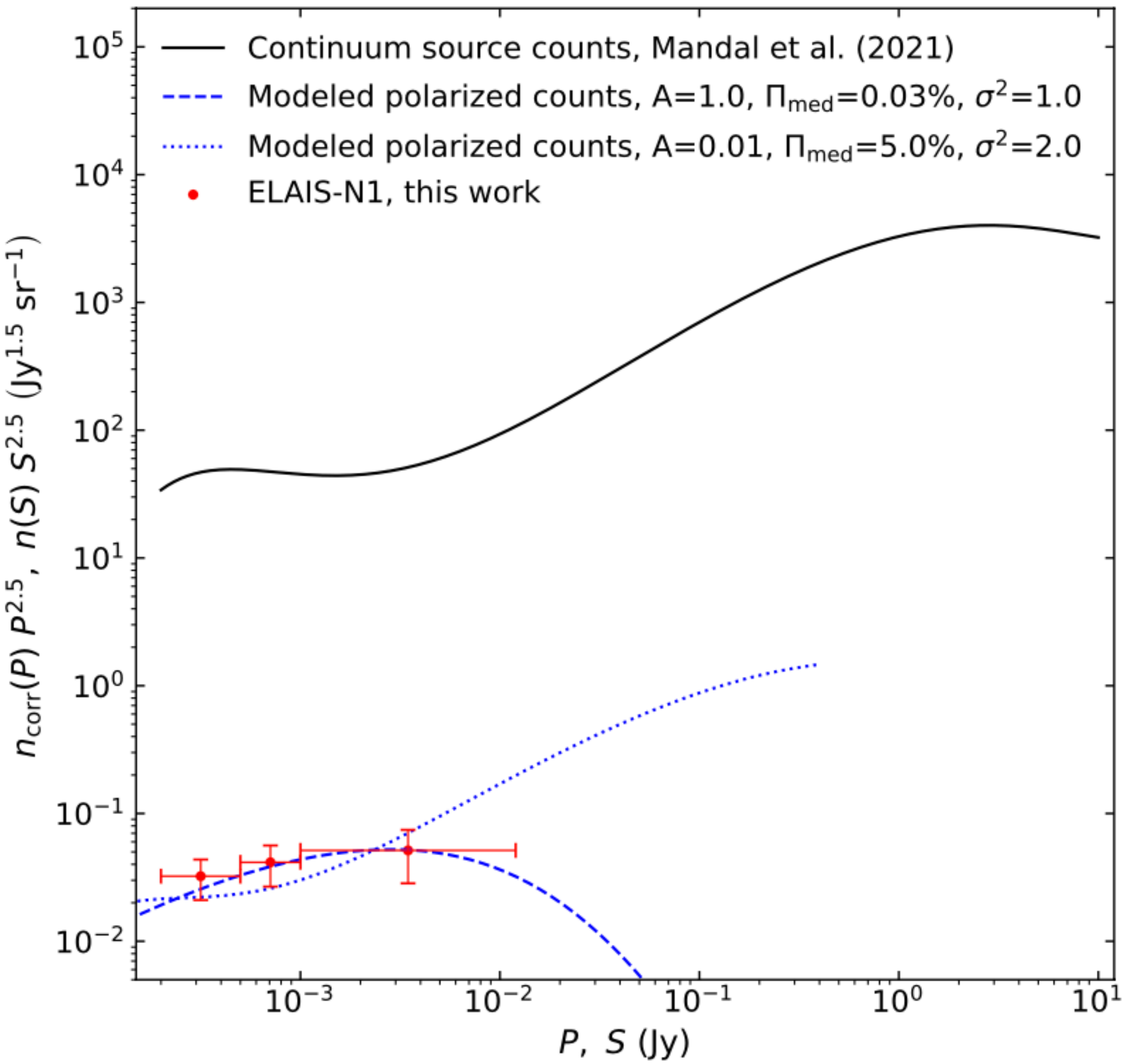

Piras et al. 2024

Counts as convolution of

- source counts in total flux density (from Mandal et al. 2021)
- with a lognormal probability function of fractional polarization

$$n(P) = A \int_{S_0=P}^{\infty} \mathscr{P}\left(\Pi = \frac{P}{S}\right)\, n(S) \frac{dS}{S}$$

$$\mathscr{P}(\Pi) = \frac{1}{\sigma\sqrt{2\pi}\Pi} \exp\left(-\frac{\left[\log(\Pi/\Pi_{\rm med})\right]^2}{2\sigma^2}\right)$$

PAPER II. ANALYSIS

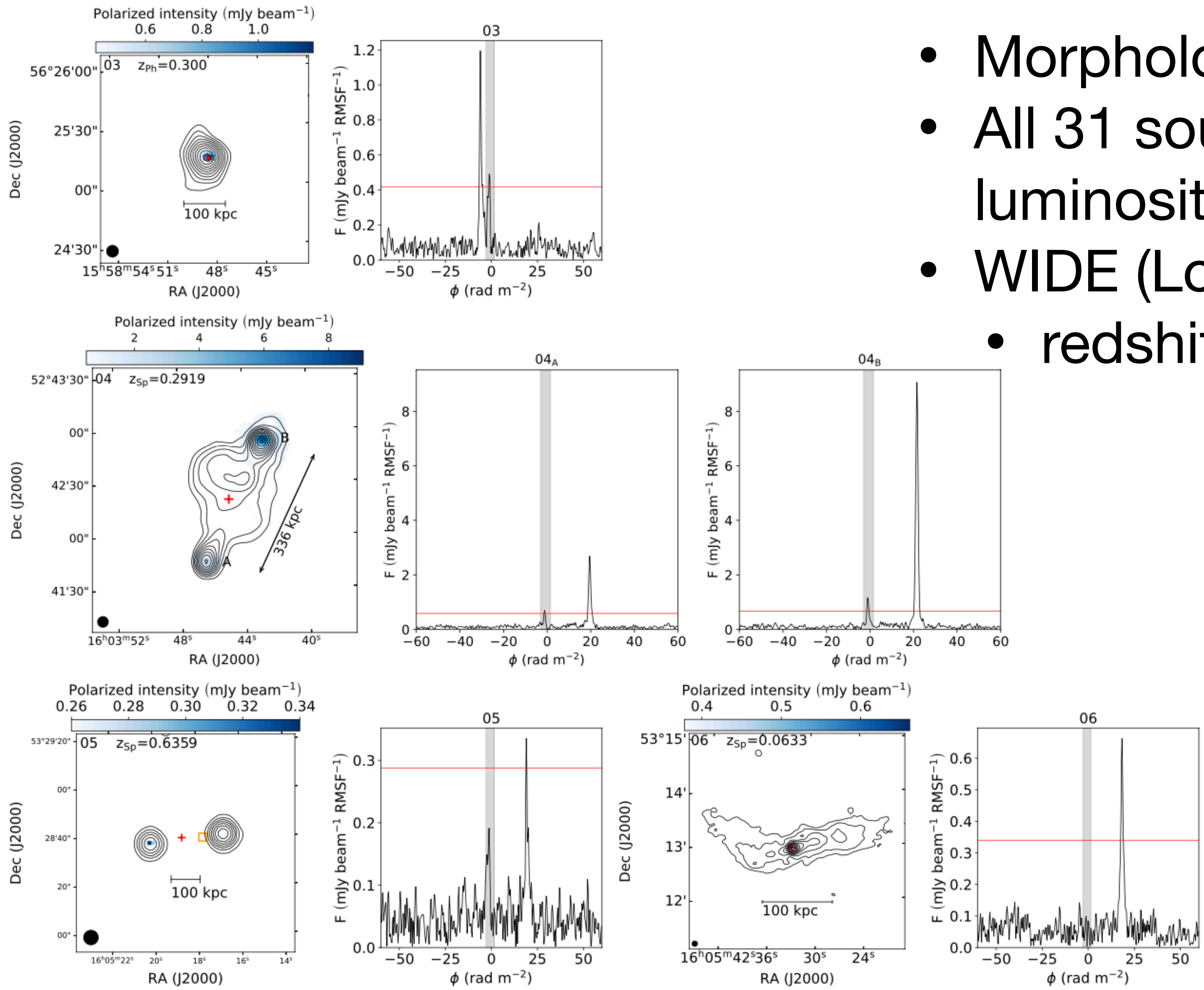

- Morphology at 150 MHz and 3 GHz
- All 31 sources with redshift (size, luminosity,…)
- WIDE (LoTSS DR2) vs DEEP (this work)
  - redshift, luminosity, RM…

Piras et al., submitted

Table 2: Radio morphological classification and some properties of the polarized radio galaxies in the ELAIS-N1 LOFAR Deep Field.

Type	N	Fraction	ID of polarized component in Paper I
Compact	4	12.9 ± 3.6%	09, 10, 24, 25
FRI	4	12.9 ± 3.6%	06, 14, 18, 32
FRII	18	58.1 ± 13.7%	01, 02, 04_A + 04_B; 05, 07, 08, 11, 12; 13^a_A + 29; 15, 17, 19, 21, 23, 26, 27^b, 30, 31^b
Other Extended	5	16.1 ± 7.2%	03, 16, 20^c, 22, 28
Total	31	100%	
Radio size > 500 kpc	9	29.0 ± 9.7%	08, 11, 12; 13_A + 29; 15, 18, 23, 26, 32
Radio size > 1 Mpc	3	9.7 ± 5.6%	11, 12, 23

PAPER II. ANALYSIS

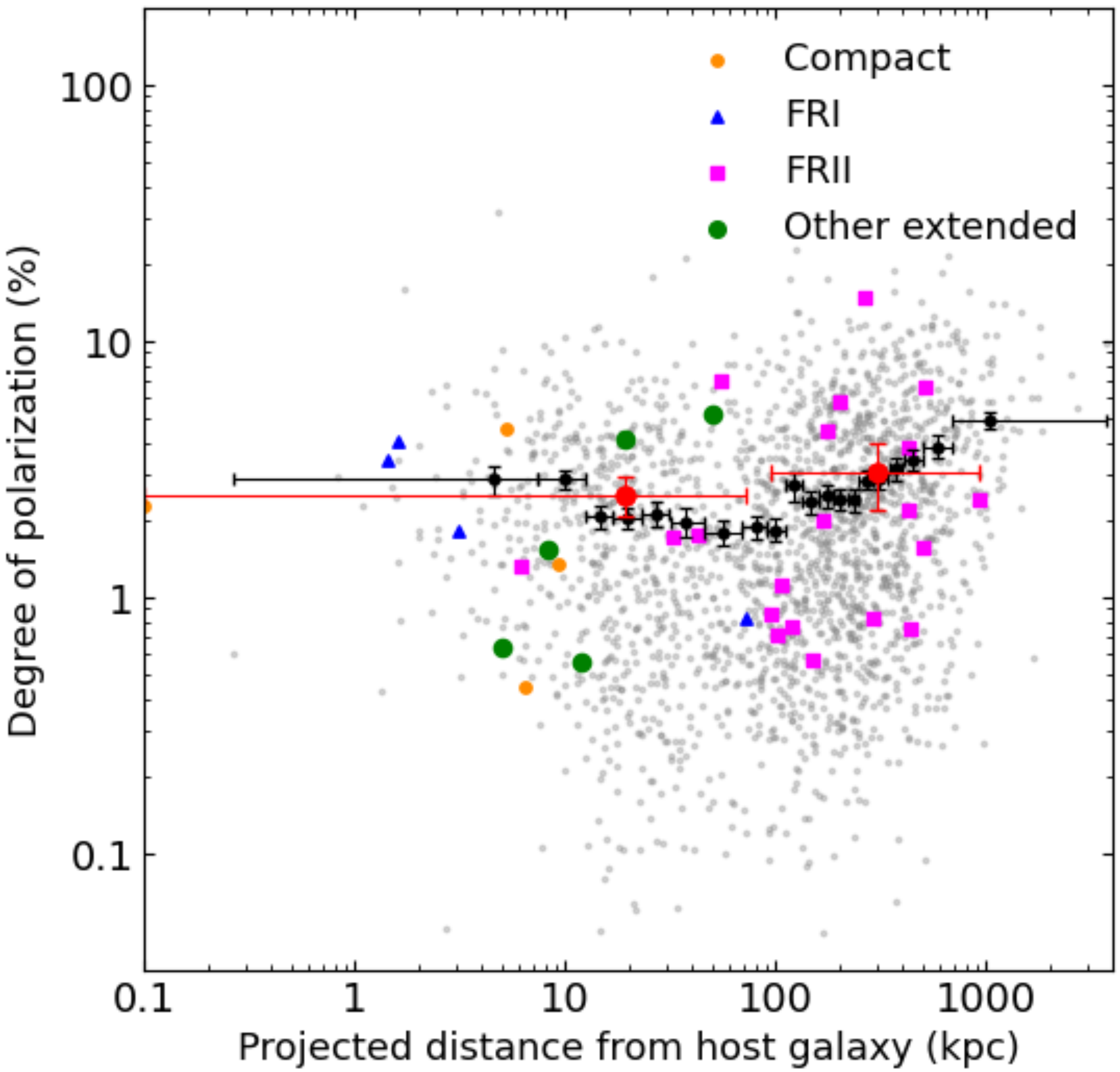

Piras et al., submitted

- **The ELAIS-N1 RM and RRM grid**

$$\mathrm{RM} = \mathrm{RM}_{\mathrm{gal}} + \mathrm{RRM}$$

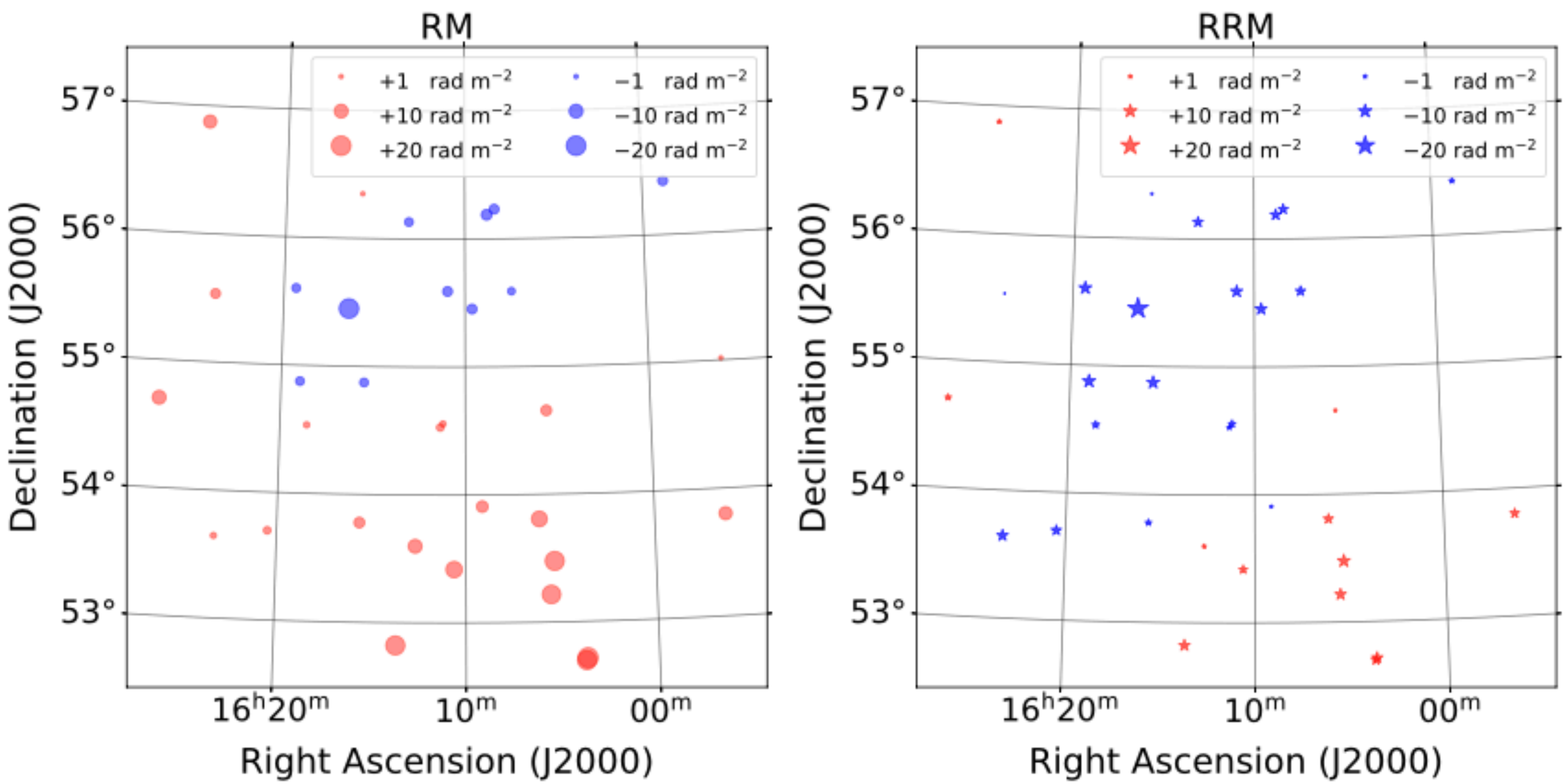

Piras et al., submitted

- **Environment**

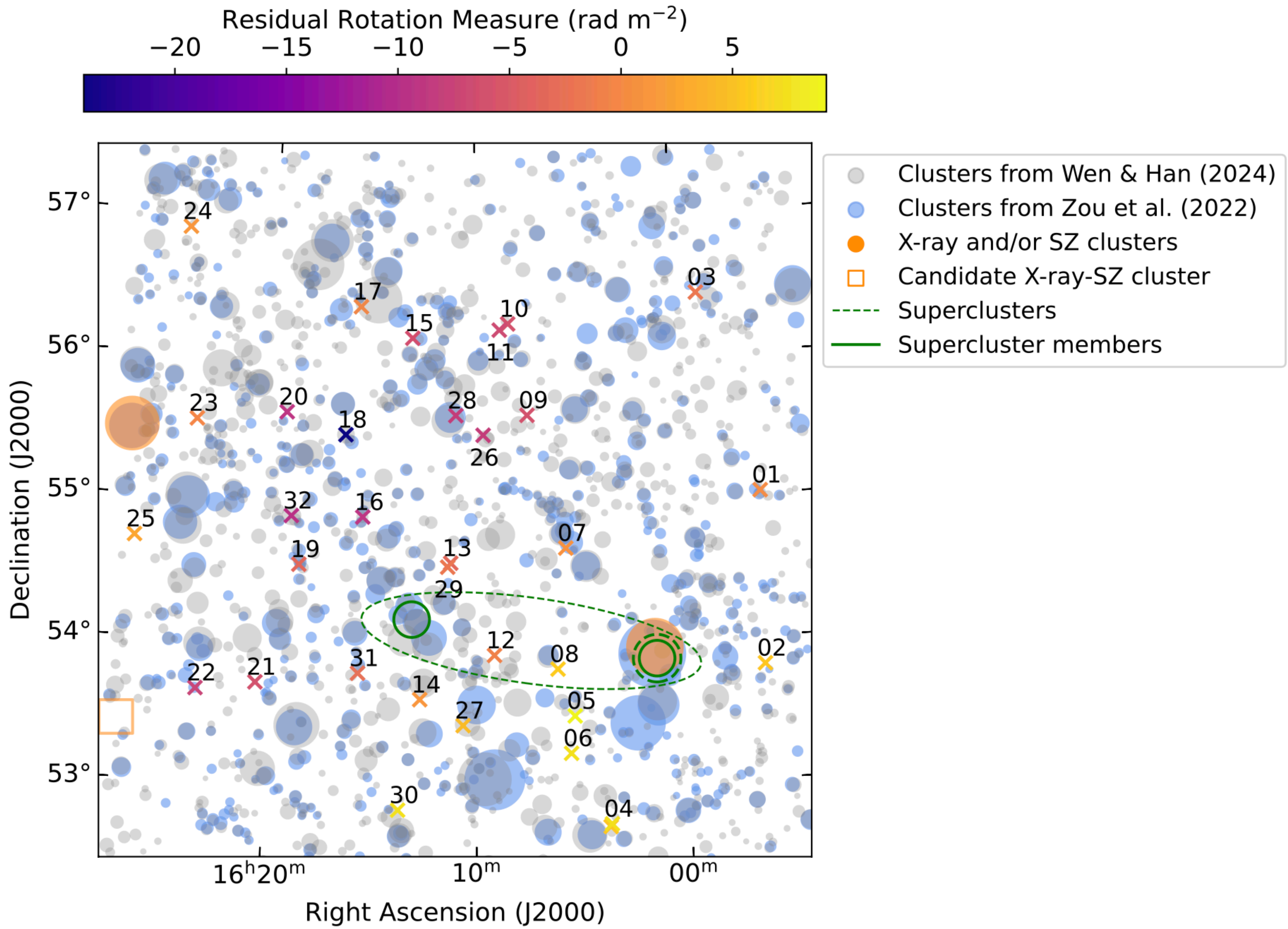

Piras et al., submitted

- **Depolarization of source 07**

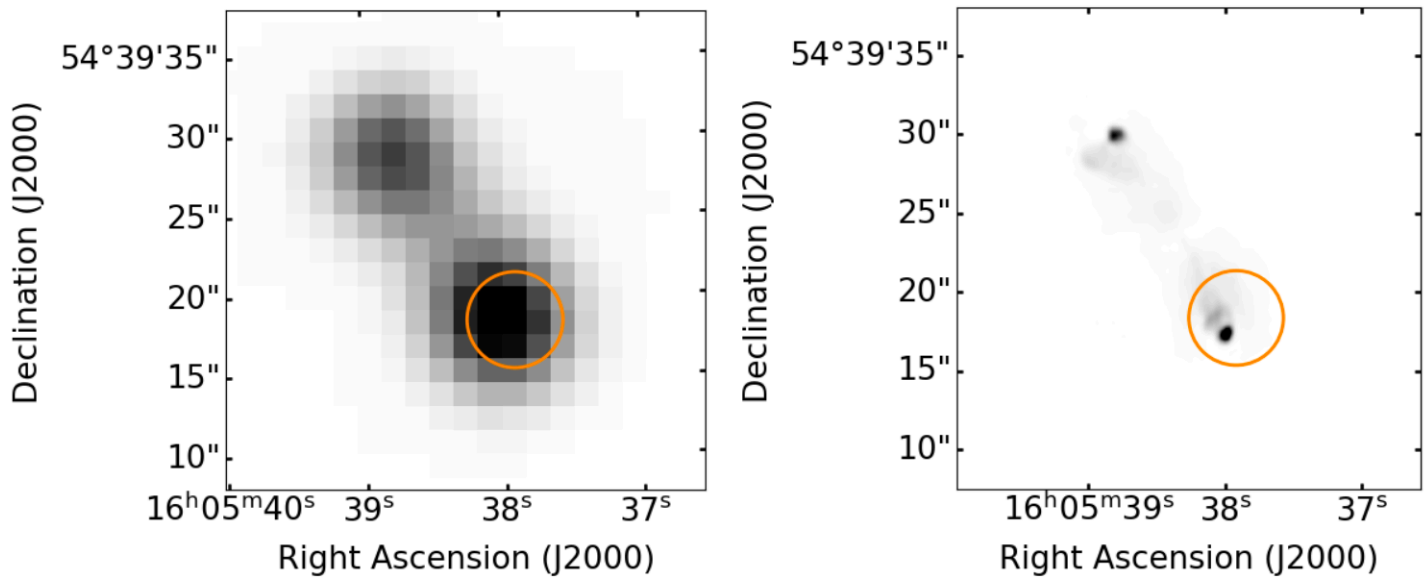

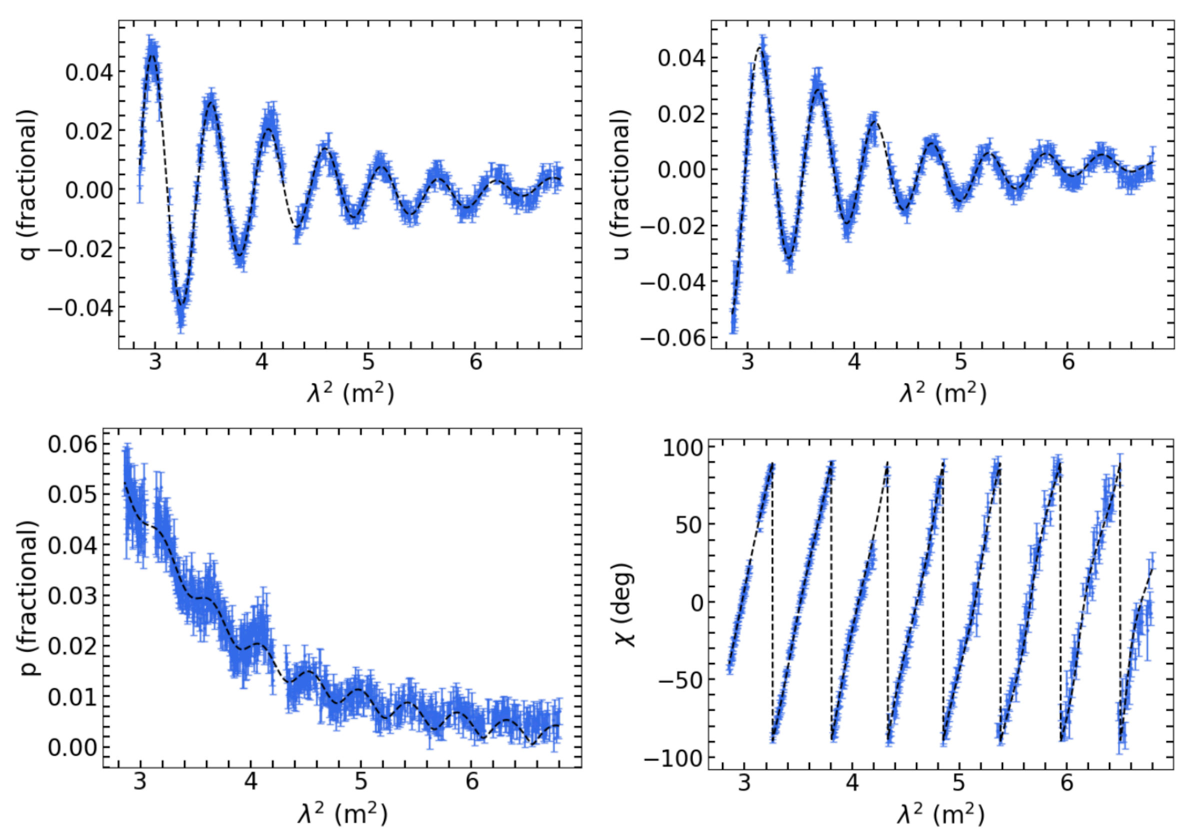

From “Polarization in the ELAIS-N1 LOFAR Deep Field”, S. Piras 2024

SUMMARY AND OUTLOOK

Paper I

- Developed new methods to stack polarization and probe the faint (sub-mJy) regime in polarization and applied them to data from ELAIS-N1
- Deepest LOFAR polarization data so far: noise level at the center of the field of 19 μJy beam^{-1}
- Detected polarization in 31 radio galaxies (1.3 polarized sources per deg^2) in the ELAIS-N1 LOFAR deep field (25 deg^2), after stacking data from 19 epochs
- Comparison with studies at 1.4 GHz
- Modelling of polarized source counts

Paper II

- Characterization of detected polarized sources
- ELAIS-N1 LOFAR deep field RM and RRM grid
- Environment of polarized sources

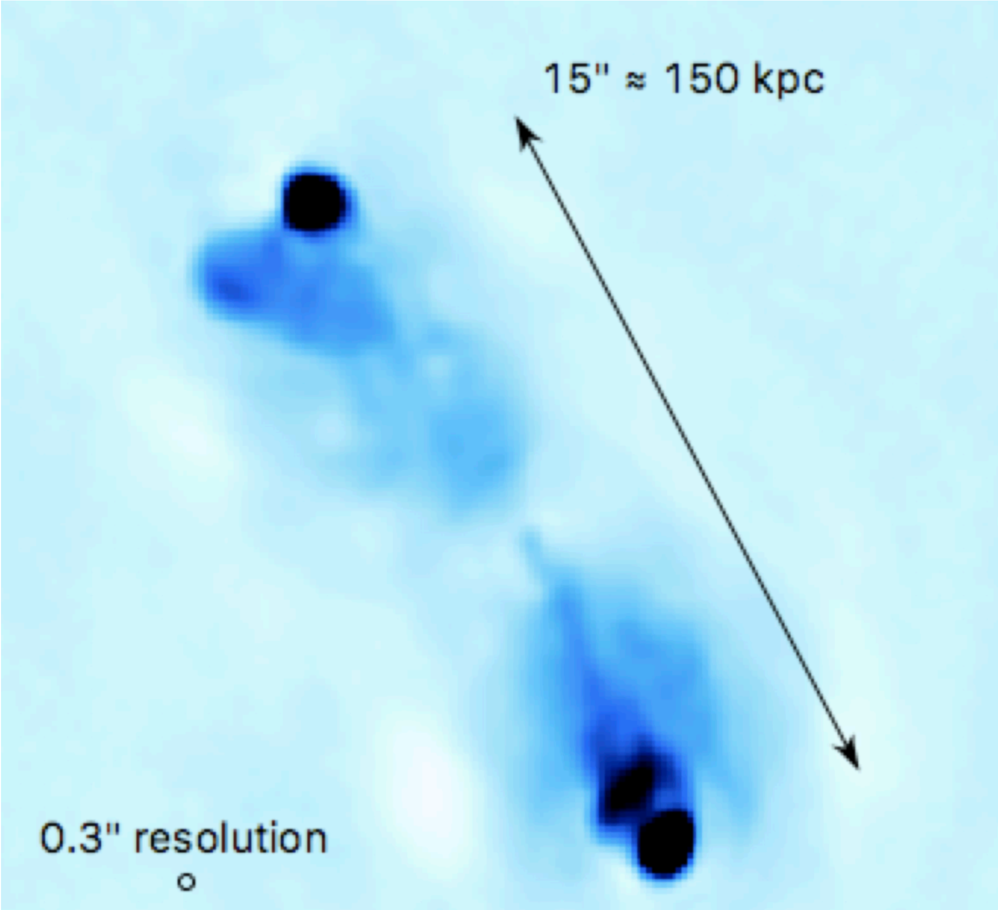

LOFAR-VLBI image (De Jong al. 2024) of source 07 of Piras et al. 2024

OUTLOOK

- **Depolarization between 1.4 GHz and 150 MHz**

Frequency	Π_{med}
1.4 GHz Grant et al. 2010	7.06%
150 MHz ∩ 1.4 GHz	1.44%
150 MHz	1.75%

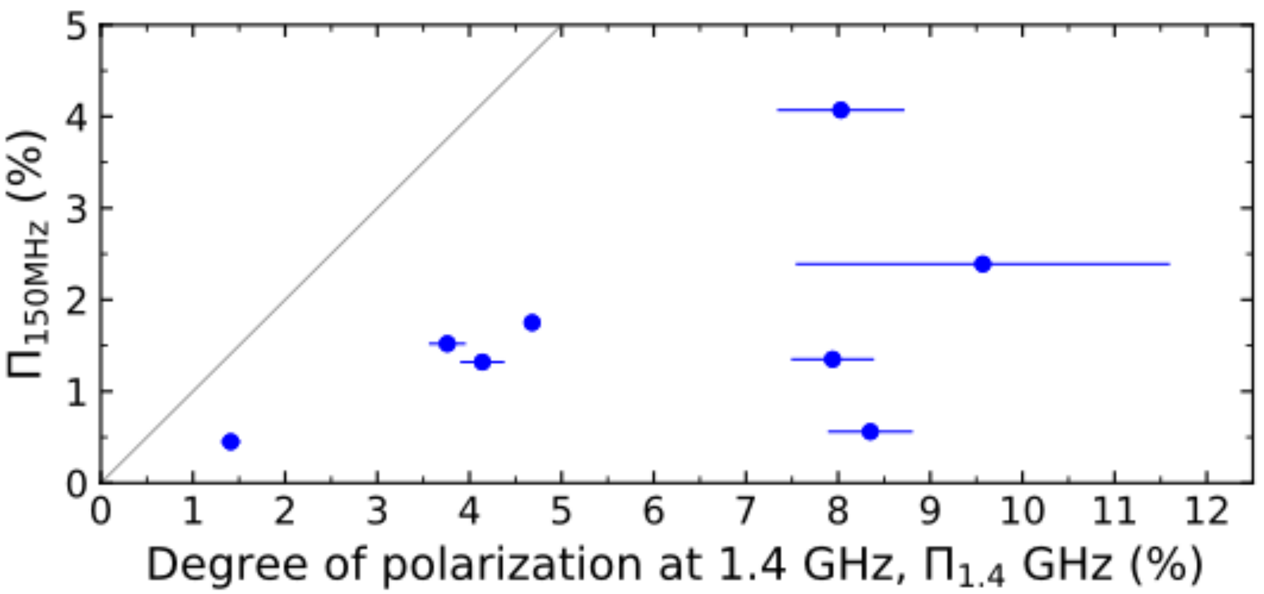

Piras et al. 2024

Probing Extragalactic Magnetic Fields

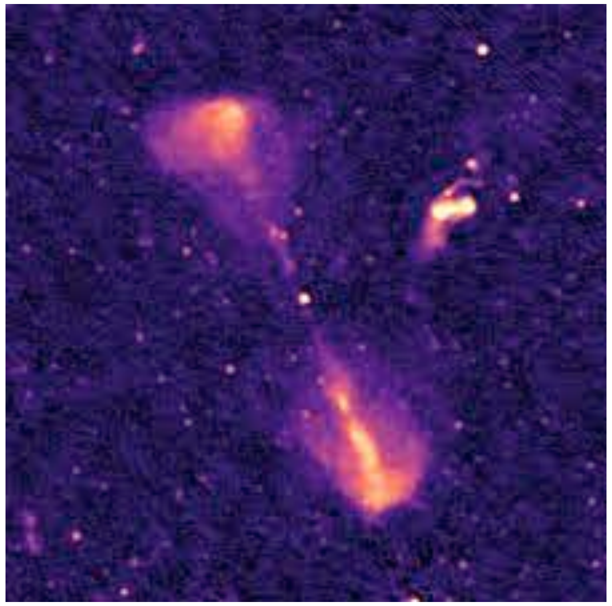

Radio galaxy observed at 150 MHz (ELAIS-N1 LOFAR deep field, Sabater et al. 2021)

Magneto-ionic medium

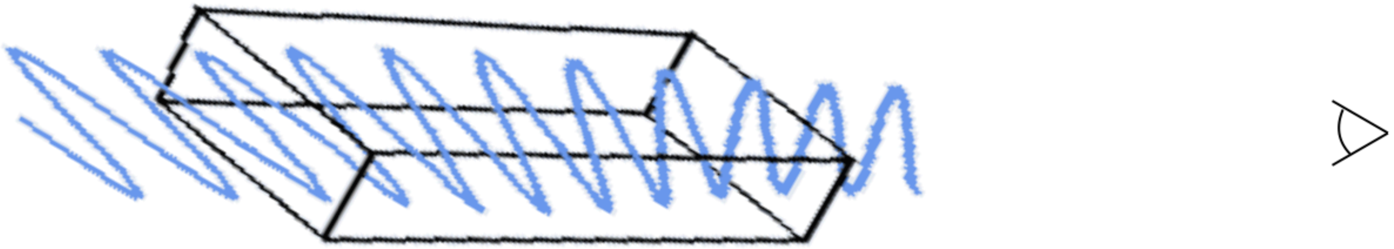

Faraday rotation of a linearly polarized emission

Faraday rotation **of linearly polarized background emission due to magneto-ionic media along the line of sight reveals indirectly magnetic fields at radio wavelengths**

Linear polarization and Stokes Parameters

$$\mathscr{P} = Q + iU = pIe^{2i\chi} = pI(\cos 2\chi + i \sin 2\chi)$$

$$\chi = \frac{1}{2} \arctan \frac{U}{Q}$$

$$p = \frac{\sqrt{Q^2 + U^2}}{I} \text{ with } 0 \leq \text{p} \leq 0.72$$

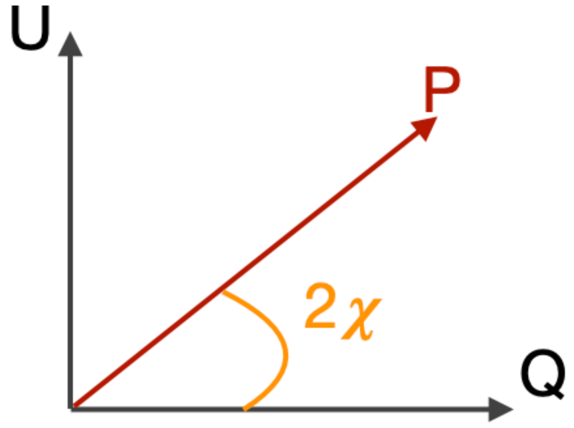

Faraday rotation measure (RM) synthesis

Frequency space ν ⟶ Faraday space ϕ

$$\mathscr{P}(\lambda^2) = \int_{-\infty}^{\infty} \mathscr{F}(\phi) e^{2i\phi\lambda^2} d\phi$$

Faraday dispersion function

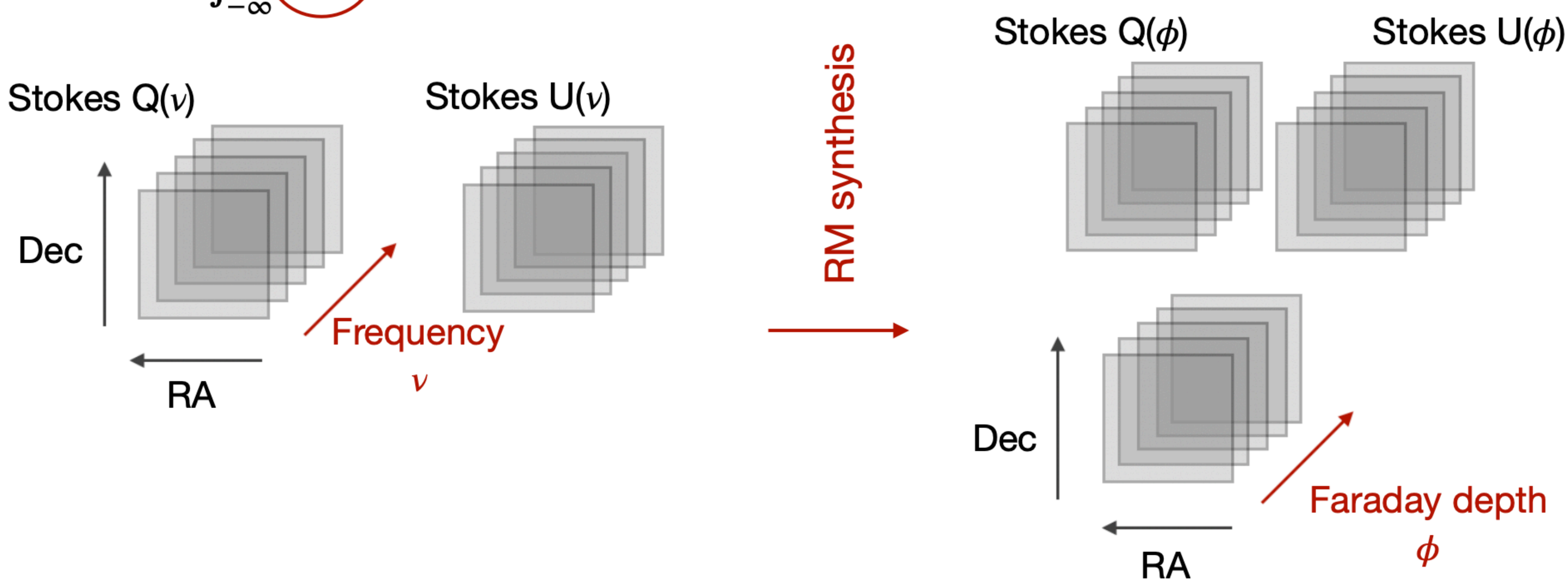

Linear polarization and Stokes Parameters

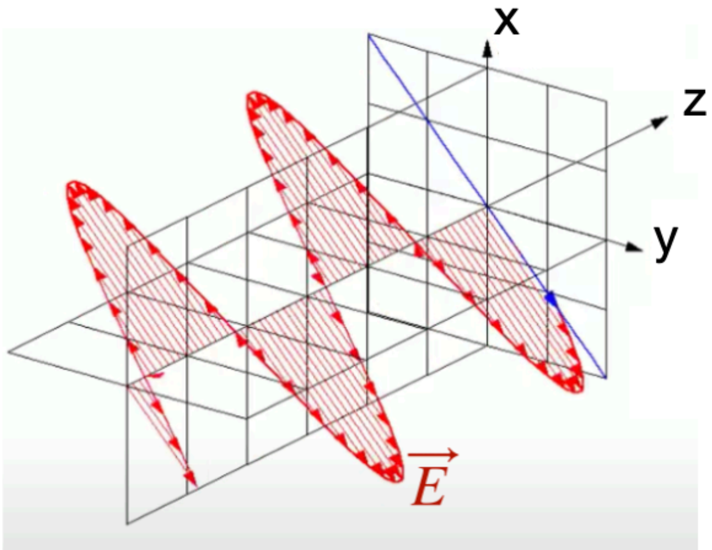

$$P = Q + iU = pIe^{2i\chi} \quad \text{with} \quad \chi = \frac{1}{2}\arctan\frac{\text{U}}{\text{Q}}$$

Complex polarization

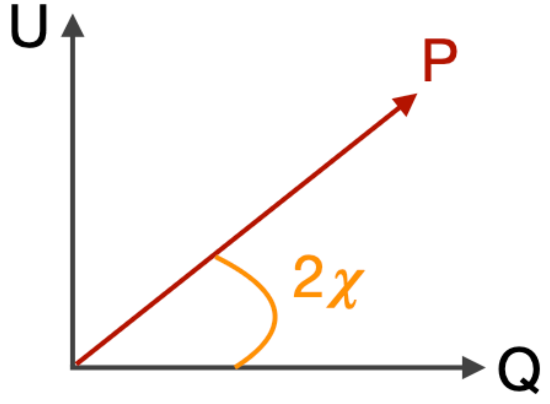

$$p = \frac{\sqrt{Q^2 + U^2}}{I} \quad with \; 0 \leq p \leq 0.72$$

χ = polarization angle

$$I = \langle E_x E_x^* \rangle + \langle E_y E_y^* \rangle$$

$$Q = \langle E_x E_x^* \rangle - \langle E_y E_y^* \rangle = \; \leftrightarrow \; - \; \updownarrow$$

$$U = \langle E_x E_y^* \rangle - \langle E_x^* E_y \rangle = \; ⤡ \; - \; ⤢$$

Stokes parameters

Depolarization

- Faraday rotation can cause a frequency-dependent reduction in the fractional polarization, and can take place inside the source, and/or it can be produced during propagation in the external medium
- Beam depolarisation 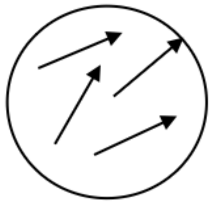

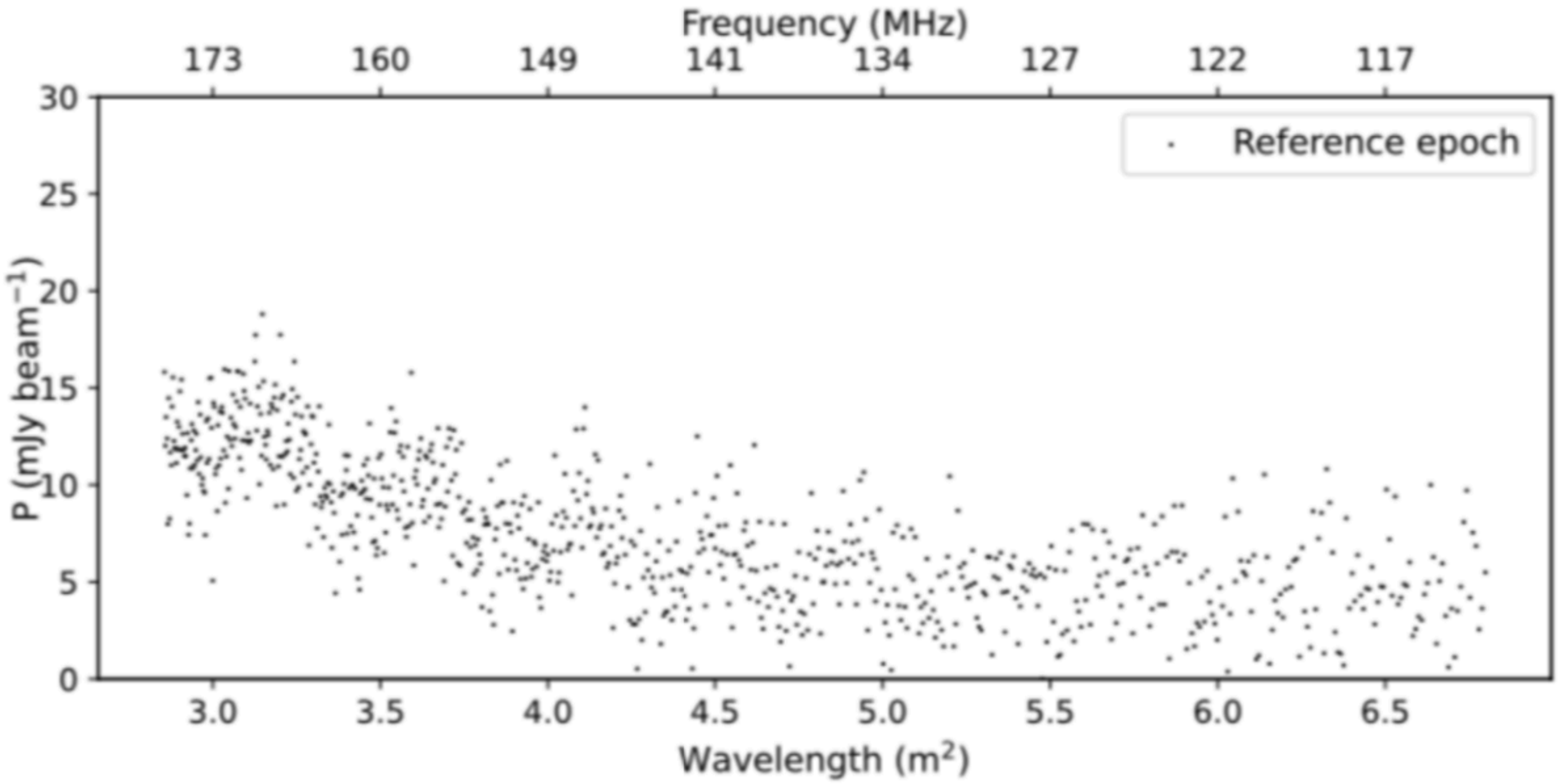

Stacking technique

Polarization angles can be different in different observing runs: it's crucial to adopt a method to align polarization angles from different epochs before stacking

Alignment in frequency space for epochs with same number of frequency channels → Reference source as calibrator: we align the polarization angle, coherently band-averaged, of the reference source of epoch to be correct with the reference polarization angle

$$\mathscr{P}^{\mathrm{corr}}_{\mathrm{Ep}}(i, j, \nu) = \mathscr{P}_{\mathrm{Ep}}(i, j, \nu)\, e^{2\mathrm{i}\Delta\chi_{\mathrm{Ep}}}$$

Herrera Ruiz et al. 2021

Alignment in Faraday depth space for cycles with different number of frequency channels →

$$\mathscr{F}^{\mathrm{corr}}_{\mathrm{Cycle\ 4}}(i, j, \phi) = \mathscr{F}_{\mathrm{Cycle\ 4}}(i, j, \phi) e^{2\mathrm{i}\phi\Delta\lambda_0^2}$$

Piras et al. 2024

Snidaric et al. 2023

Stacking technique

Polarization angles can be different in different observing runs: it's crucial to adopt a method to align polarization angles from different epochs before stacking

Alignment in 2 steps:

1. **in frequency space for epochs with same number of frequency channels**
2. in Faraday depth space for cycles with different number of frequency channels

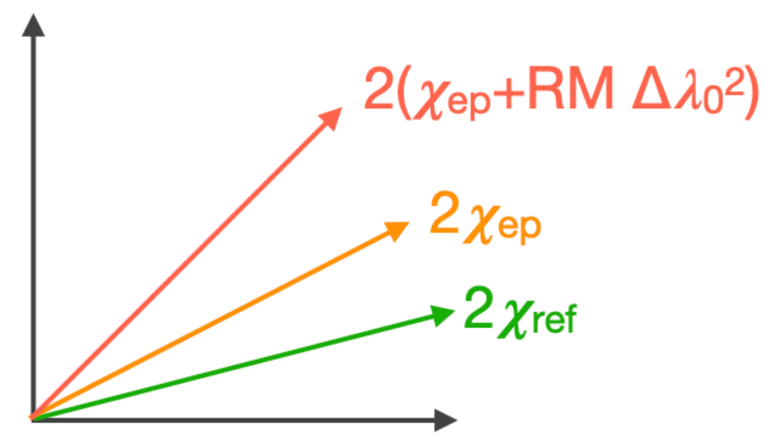

$$\chi = \frac{1}{2} \arctan \frac{U(\nu)}{Q(\nu)}$$

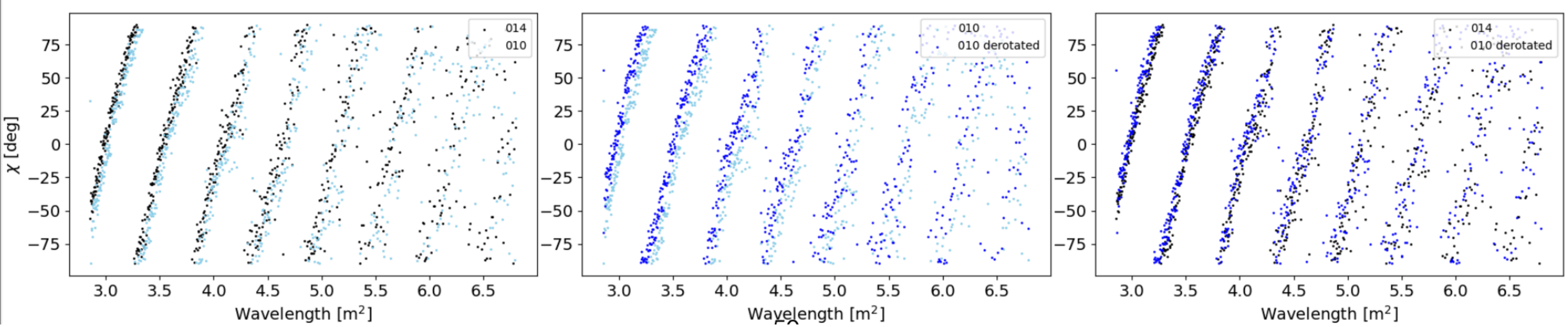

Piras et al. 2024

Stacking technique

Polarization angles can be different in different observing runs: it’s crucial to adopt a method to align polarization angles from different epochs before stacking

Alignment in 2 steps:

Piras et al. 2024

1. in frequency space for epochs with same number of frequency channels
2. **in Faraday depth space for cycles with different number of frequency channels**

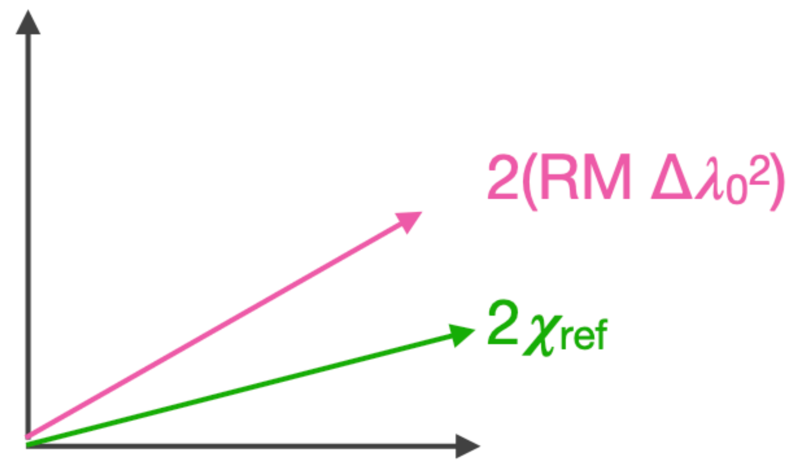

$$\chi = \frac{1}{2} \arctan \frac{U(\phi)}{Q(\phi)}$$

Stacking technique

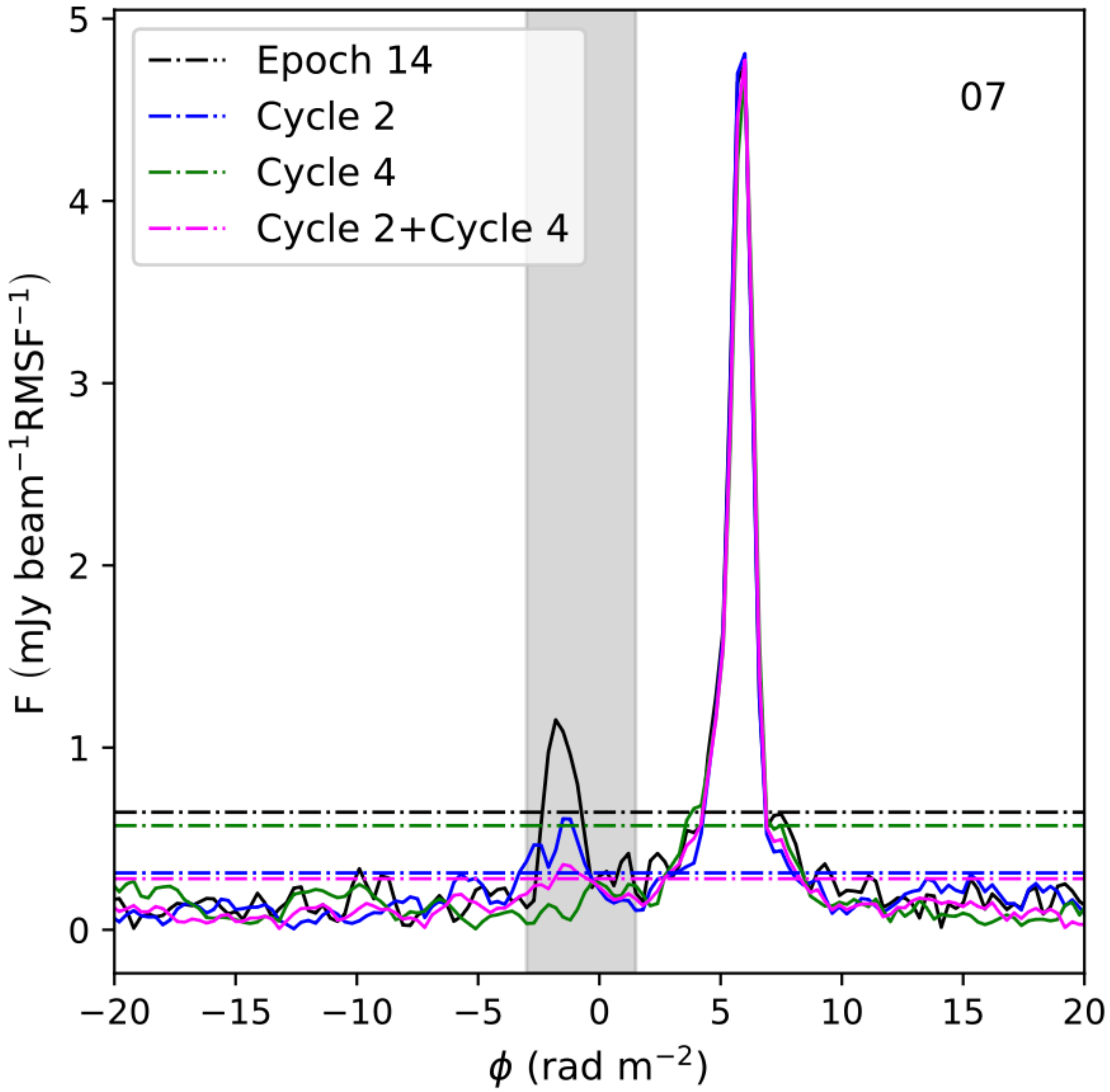

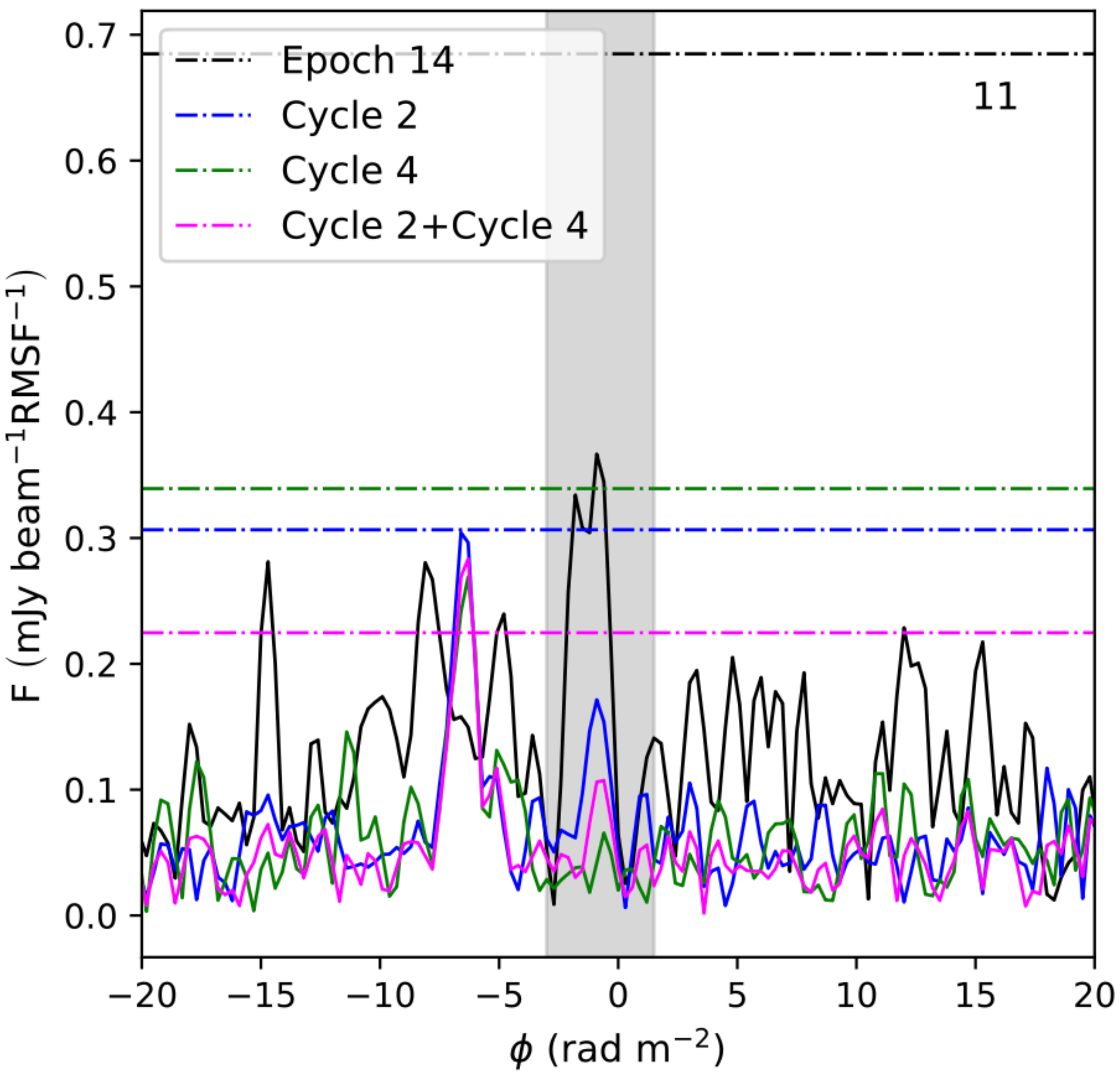

Piras et al. 2024

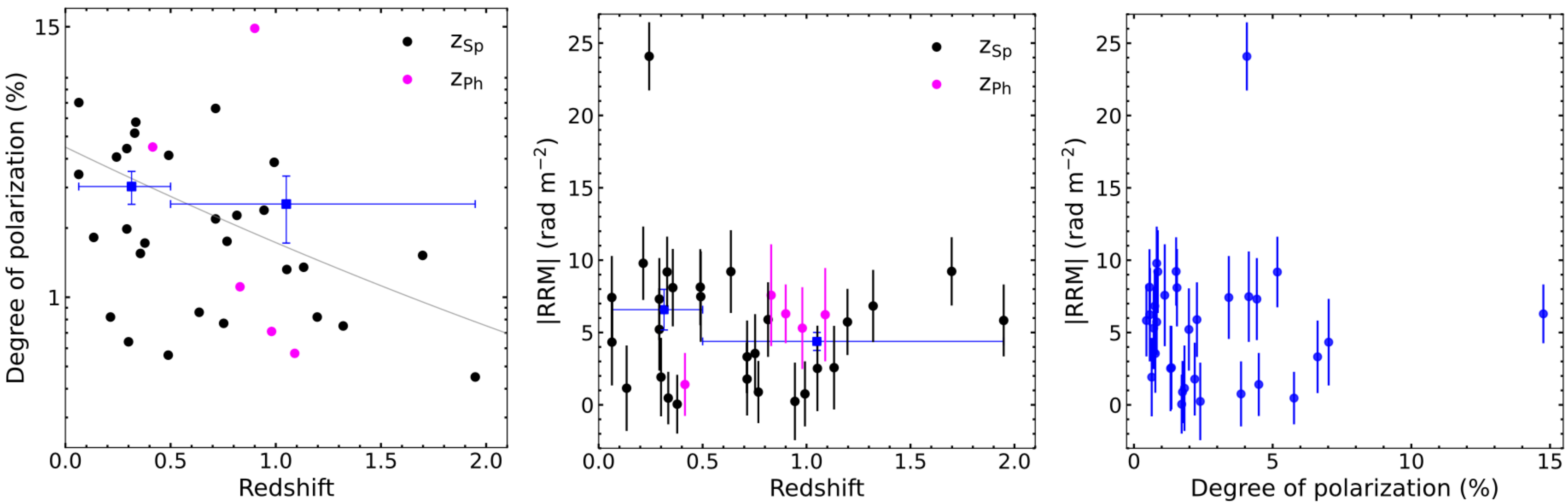

Piras et al., submitted